Halogen activation in the plume of Masaya volcano: field observations and box model investigations

Julian Rüdiger[1,10], Alexandra Gutmann[1], Nicole Bobrowski[2,3], Marcello Liotta[4], J. Maarten de Moor[5], Rolf Sander[3], Florian Dinger[2,3], Jan-Lukas Tirpitz[2], Martha Ibarra[6], Armando Saballos[6], María Martínez[5], Elvis Mendoza[6], Arnoldo Ferrufino[6], John Stix[7], Juan Valdés[8], Jonathan M. Castro[9], and Thorsten Hoffmann[1]

[1]Johannes Gutenberg-University, Institute of Inorganic and Analytical Chemistry, Mainz, Germany
[2]Institute for Environmental Physics, University of Heidelberg, Heidelberg, Germany
[3]Max-Planck Institute for Chemistry, Mainz, Germany
[4]Istituto Nazionale di Geofisica e Vulcanologia, Sezione di Palermo, Italy
[5]Observatorio Vulcanológico y Sismológico de Costa Rica Universidad Nacional, Heredia, Costa Rica
[6]Instituto Nicaragüense de Estudios Territoriales, Nicaragua
[7]Department of Earth and Planetary Sciences, McGill University, Montreal, Canada
[8]Laboratorio de Química de la Atmósfera, Universidad Nacional, Heredia, Costa Rica
[9]Institute of Geosciences, Johannes Gutenberg University Mainz, Mainz, Germany
[10]Chair of Environmental Chemistry and Air Research, Technical University Berlin, Berlin, Germany

Correspondence to: Thorsten Hoffmann (t.hoffmann@uni-mainz.de)

Abstract. Volcanic emissions are a source of halogens in the atmosphere. Rapid reactions convert the initially emitted hydrogen halides (HCl, HBr, HI) into reactive species e.g. BrO, Br_2, BrCl, ClO, OClO and IO. The activation reaction mechanisms in the plume consume ozone (O_3), which is entrained by mixed in ambient air. In this study, we present observations of the oxidation of bromine, chlorine and iodine during the first 11 minutes after emission, examining the plume from Santiago Crater of Masaya volcano in Nicaragua. Two field campaigns were conducted, in July 2016 and September 2016. The sum of the reactive species of each halogen was determined by gas diffusion denuder sampling followed by GC-MS analysis, while the total amounts of halogens and sulfur amounts were obtained by alkaline trap sampling with subsequent IC and ICP-MS measurements. Both ground and airborne sampling with an unoccupied aerial vehicle (carrying a denuder sampler in combination with an electrochemical SO_2 sensor) were conducted at varying distances from the crater rim. The in-situ measurements were accompanied by remote sensing observations (DOAS). The reactive fraction of bromine increased from 0.20 ± 0.13 at the crater rim to 0.76 ± 0.26 at 2.8 km downwind, while chlorine showed an increase of the reactive fraction from $(2.7\pm0.7)\times10^{-4}$ to $(11\pm3)\times10^{-4}$ in the first 750 m. Additionally, a reactive iodine fraction of 0.3 at the crater rim and 0.9 at 2.8 km was measured. No significant change in BrO/SO_2 molar ratios was observed with the estimated age of the observed plume ranging from 1.4 min to 11.1 min. This study presents a large complementary data set of different halogen compounds at Masaya volcano that allowed the quantification of reactive bromine in the plume of Masaya volcano at different plume ages. With the observed field data, a chemistry box model (CAABA/MECCA) allowed us to reproduce the observed trend in the

ratio of the reactive bromine to total bromine ratio. An observed contribution of BrO to the reactive bromine fraction of about 10 % was reproduced in the first few minutes of the model run.

1. Introduction

Volcanoes are known to be important emitters of atmospheric trace gases and aerosols, both through explosive eruptions and persistent quiescent degassing (von Glasow et al., 2009). The most abundant gases in volcanic emissions are water, carbon dioxide, sulfur compounds and hydrogen halides (Symonds et al., 1994). Typically, halogen emissions are largely dominated by chlorine (HCl) and fluorine (HF), while bromine (HBr) and iodine (HI) are three and five orders of magnitude less abundant than chlorine and fluorine, respectively (e.g., Aiuppa et al., 2005; Pyle and Mather, 2009). Despite their low abundance, the heavy halogens (bromine and iodine) can have significant impact on the chemistry of the atmosphere (e.g., von Glasow, 2010; Saiz-Lopez and von Glasow, 2012; Platt and Bobrowski, 2015). The chemical composition of volcanic plumes is the subject of a large number of studies, often aimed at gaining insights into subsurface processes, such as the degassing of magma in connection with changes in volcanic activity (e.g., Aiuppa et al., 2007). In addition, the effects of volcanic gases on the atmosphere and biosphere at local, regional and global scales are also of interest, e.g., acid deposition (wet and dry), nutrient input (e.g., Delmelle, 2003), aerosol formation and effects on the solar radiation balance (e.g., Mather et al., 2013; Malavelle et al., 2017).

Volcanic halogen emissions have been studied for years (e.g., Noguchi and Kamiya, 1963; Giggenbach, 1975) and the determination of chlorine and sulfur is a common procedure in such gas geochemical investigations. Bromine only attracted more attention in later years, when the reactive bromine species BrO was observed in volcanic plumes (e.g., Bobrowski et al., 2003; Oppenheimer et al., 2006). This also proved that not only sulfur species (H_2S, SO_2) undergo oxidation by ambient reactants (such as OH, O_3), and laid the basis for various studies on oxidized halogen species (BrO, ClO, OClO, IO) (e.g., Lee et al., 2005; Theys et al., 2014; General et al., 2015; Gliß et al., 2015; Schönhardt et al., 2017). Despite the low abundance of bromine in volcanic gas emissions, the relatively simple detection of BrO by differential optical absorption spectroscopy (DOAS) promoted research on the origin and fate of BrO in volcanic plumes. Based on thermodynamic modelling, Gerlach (2004) hypothesized that BrO is not primarily emitted by volcanoes, but is formed only after the initial emissions are mixed with entrained ambient air. Since SO_2 can also be easily measured by DOAS and the oxidation of SO_2 plays a minor role over period of minutes to hours (McGonigle et al., 2004), the ratio of BrO to SO_2 is used as a dilution-compensated observation parameter.

An increase in the BrO/SO_2 ratio with increasing distance from the emitting vent was observed at various volcanoes (e.g., Bobrowski et al., 2007; Vogel, 2012; Gliß et al., 2015), together with variations of BrO/SO_2 in a lateral plume dimension with higher ratios at the edges of the plume (e.g., Bobrowski et al., 2007; Louban et al., 2009; General et al., 2015; Kern and Lyons, 2018). This was explained by a limited transfer of atmospheric O_3 to the center of the plume, which is thought to promote the formation of BrO in a chain reaction mechanism involving heterogeneous chemistry. Shortly after the discovery of the reactive bromine species BrO, reactive chlorine species, ClO and OClO, were also observed using the same DOAS techniques (e.g., Lee et al., 2005; Bobrowski et al., 2007; Donovan et al., 2014; Theys et al., 2014; General et al., 2015; Gliß et al., 2015, Kern and Lyons, 2018). It was found that the abundance of ClO and OClO is on the same order of magnitude as BrO, in contrast to total chlorine, which is typically three orders of magnitude more abundant than bromine. The formation of reactive chlorine species is considered to be a secondary product of the activation cycle of bromine (see Table 1). Recently, reactive iodine species have also been detected by satellite observations in the plume of Kasatochi (Schönhardt et al., 2017), but could not be confirmed by ground-based measurements so far.

Both the transformation of halogen species in the plume and their fate in the atmosphere are of interest. In particular, the clarification of the question of the amounts emitted into the atmosphere and the distribution of the halogens emitted by quiescent (i.e., passive, non-eruptive) and eruptive degassing are of interest. The global volcanic SO_2 flux has been estimated as 23 Tg/yr for the period from 2004-2016 (Carn et al., 2017), resulting in estimated halogen fluxes of the same order for chlorine and three orders of magnitude lower for bromine, taking into account global mean sulfur/halogen ratios (Aiuppa et al., 2009).

Bromine from various sources (e.g. polar regions, salt lakes, volcanoes) is involved in tropospheric and stratospheric ozone depletion (e.g., Wennberg, 1999; Rose et al., 2006; Simpson et al., 2007). Tropospheric ozone depletion has also been observed in volcanic plumes (e.g., Hobbs et al., 1982; Kelly et al., 2013; Surl et al., 2015; Roberts, 2018), which supports the proposed reaction mechanisms for BrO formation via autocatalytic chain reactions. Recent observations of halogen oxides by satellites (e.g., Theys et al., 2009; Carn et al., 2016) and aircraft missions (Heue et al., 2011) confirm that some large volcanic eruptions may inject a proportion of their volcanic halogens into the free troposphere or even to the stratosphere and therefore their potential impact on stratospheric ozone. In addition to effects of volcanic degassing on atmospheric chemistry, measurements of volcanic emission have become an important and well-established tool in the assessment of volcanic hazard, and gas monitoring is used at many volcanoes around the world (e.g., Carroll and Holloway, 1994; Aiuppa et al., 2007; de Moor et al., 2016).

It has been also observed that the BrO/SO_2 gas ratio changes with the activity of volcanoes. Bobrowski and Giuffrida (2012) observed lower BrO/SO_2 ratios in Etna’s plume during eruptive phases. Also long-term observations using DOAS by Lübcke et al. (2014), who used stationary spectrometers within the NOVAC network (Galle et al., 2010), showed a decrease in the BrO/SO_2 ratio before and during explosive activity at Nevado del Ruiz volcano. More recently, a study by Dinger et al. (2018) at the Cotopaxi volcano (Ecuador) showed low BrO/SO_2 ratios at the beginning of eruptive activity compared to higher ratios present during declining volcanic activity. Finally, Warnach et al. (2019) found low BrO/SO_2 ratio during high explosive periods and an increased BrO/SO_2 ratio during less explosive periods at Tungurahua volcano.

However, it is not clear yet whether the BrO/SO_2 ratio can be used as a robust diagnostic tool for forecasting volcanic activity. Since BrO is a reactive secondary gas species, its concentration in a volcanic plume potentially depends on atmospheric variables such as humidity, oxidant abundance, solar radiation, and aerosol surface. The BrO/SO_2 ratio might not always or only partially be controlled by the total bromine emission at a particular volcano under study (Roberts et al., 2018). Further knowledge of the chemistry that drives halogen activation is therefore required.

After the introduction, the article starts in section 2 with an overview of the volcanic plume halogen chemistry and relating model studies. It then presents our comprehensive data set obtained during two field campaigns at Masaya volcano using several measurement techniques, including DOAS (e.g, Bobrowski et al., 2003), MultiGAS (Shinohara, 2005; Aiuppa et al., 2006), alkaline trap (e.g., Wittmer et al., 2014) and gas diffusion denuder sampling (e.g., Rüdiger et al., 2017) (see section 3) The use of an unoccupied aerial vehicle (UAV) (e.g., Rüdiger et al., 2018; Stix et al., 2018) enabled the sampling of a downwind plume for the investigation of halogen-induced plume aging processes, which is reproduced by atmospheric modelling of plume halogen chemistry (see section 4). In section 5 the outcome of the modelling is compared with the field measurement results before section 6 draws the conclusions and provides an outlook for future studies.

2. Volcanic plume halogen chemistry

Besides numerous field surveys at various volcanoes, several atmospheric modelling studies have been conducted, which have improved our understanding of the complex chemical reactions in volcanic plumes marking the interface between volcanic trace gases (and aerosols) and ambient air. Two different models have been developed by researchers to simulate the in-plume chemistry, MISTRA (Bobrowski et al., 2007; von Glasow, 2010) and PlumeChem (Roberts et al., 2009; Roberts et al., 2014). While MISTRA is a one-dimensional box model including multiphase chemistry, PlumeChem additionally includes plume dispersion and 3D simulation by employing a multiple grid box mode, while the multi-phase chemistry is parameterized using uptake coefficients rather than being modelled explicitly in the aqueous phase. The models (MISTRA, PlumeChem and also the here used CAABA/MECCA) are initialized with the gas composition of a so-called "effective source region". This gas composition is typically derived from a thermodynamic equilibrium model (HSC) (e.g., Gerlach, 2004; Martin et al., 2006). Different mixtures of magmatic gas and ambient air yield the hot gas mixture of the "effective source region", which is quenched to ambient temperature and then mixed with ambient air including O_3, OH and NO_X. The suitability of the HSC model to represent high-temperature chemistry in the plume has been debated and recently it has been shown that the chemistry should be better represented by kinetics model (Martin et al., 2012; Roberts et al., 2019). The limitations of HSC to represent the high-temperature chemistry include the assumption of thermodynamic equilibria in the hot plume region, which is quite improbable. The choices for temperature, a mixing ratio of volcanic and magmatic gas, and a 'quenching factor' are rather arbitrary and do not necessarily reflect reality. The kinetics model studies show that the timescale for substantial NO_x to be formed thermally appears longer than a reasonable lifetime of a hot plume (Martin et al., 2012). Whilst Roberts et al. 2019 shows differences in the predicted formation of H_xO_y in a kinetics model compared to those assumed by thermodynamics, in terms of magnitudes and speciation. Therefore, conclusions drawn from atmospheric modelling that depends on the HSC initializations are inherently limited by the uncertainties and limitation of HSC. Nevertheless, we follow here the former studies using HSC, despite of its limitation, because at the moment there is no full kinetics model with CHONS-halogens chemistry available as an alternative.

The initially emitted HBr is converted into reactive species via an autocatalytic mechanism, involving multiphase reactions, which constitute so-called "bromine explosion" (von Glasow et al., 2009). Under ozone consumption, Br radicals – formed by high temperature dissociation in the "effective source region" – react to BrO (Table1, R1), which in turn reacts with HO_2 or NO_2 to form HOBr (R2) or $BrNO_3$, respectively. A subsequent uptake into aerosol enables the conversion of HBr into Br_2, which partitions into the gas phase and is photolyzed to give two Br radicals and start the cycle again (R5a). The self-reaction of two BrO to give two Br (with Br_2 as a secondary product) and O_2 is suggested to be the major ozone-depleting channel at high bromine concentrations as in a young plume (von Glasow 2009). Once HBr becomes depleted, the uptake of HOBr/$BrNO_3$ may promote the formation of BrCl, which also consumes O_3 and forms reactive chlorine species such as ClO and OClO (R6, R8). The major reaction pathways that involve the formation and degradation of BrO in volcanic plumes are shown in Table1. An extensive review of the advances of bromine speciation in volcanic plumes including a comparison of different model approaches has recently been presented by Gutmann et al (2018). In this study, we present in situ measurements along with remote sensing data on the activation of Br, Cl and I in the volcanic plume of Masaya and further investigate the involved halogen species by atmospheric model simulations using the CAABA/MECCA box model. Although fluorine has been measured as well, it is not discussed in detail in this study, due to the high water solubility and the non-reactivity of fluoride towards oxidation.

Table 1: Overview on halogen reactions in volcanic plumes (X = Cl, Br)

$Br_{(g)} + O_{3(g)} \rightarrow BrO_{(g)} + O_{2(g)}$	(R1)
$BrO_{(g)} + HO_{2(g)} \rightarrow HOBr_{(g)} + O_{2(g)}$	(R2)
$HBr_{(g)} \rightarrow Br^{-}_{(aq)} + H^{+}_{(aq)}$	(R3)
$HOBr_{(aq)} + Br^{-}_{(aq)} + H^{+}_{(aq)} \rightarrow Br_{2(g)} + H_2O_{(aq)}$	(R4a)
$HOBr_{(aq)} + HCl_{(aq)} \rightarrow BrCl_{(g)} + H_2O_{(aq)}$	(R4b)
$Br_{2(g)} \xrightarrow{h\nu} 2\ Br_{(g)}$	(R5a)
$BrCl_{(g)} \xrightarrow{h\nu} Br_{(g)} + Cl_{(g)}$	(R5b)
$Cl_{(g)} + O_{3(g)} \rightarrow ClO_{(g)} + O_{2(g)}$	(R6)
$BrO_{(g)} + BrO_{(g)} \rightarrow 2\ Br_{(g)} + O_{2(g)}$	(R7a)
$BrO_{(g)} + BrO_{(g)} \rightarrow Br_{2(g)} + O_{2(g)}$	(R7b)
$BrO_{(g)} + ClO_{(g)} \rightarrow OClO_{(g)} + Br_{(g)}$	(R8)
$BrO_{(g)} + NO_{2(g)} \rightarrow BrONO_{2(g)}$	(R9)
$BrONO_{2(g)} + H_2O_{(aq)} \rightarrow HOBr_{(aq)} + HNO_{3(aq,g)}$	(R10)

3. Measurements

3.1. Site description and flight/sample strategy

Masaya volcano in Nicaragua is a shield volcano with a caldera size of 6 km x 11 km. The caldera hosts a set of vents, of which the Santiago pit crater, that formed in 1858-1859, is currently active (McBirney, 1956). Since mid-November 2015, Santiago crater has contained a persistent superficial lava lake (~40 m x 40 m). The lava lake has been associated with large volcanic gas emissions, making it one of the largest contributors in SO_2 emissions of the Central American volcanic arc (Martin et al., 2010; de Moor et al., 2017; Aiuppa et al., 2018). Due to high emission rates and the low-altitude ground-hugging plume, Masaya volcano has a severe environmental impact on the downwind areas, affecting human and animal health and vegetation (Delmelle et al., 2002; van Manen, 2014). With its easy accessibility by car and low altitude, the emissions of Masaya volcano have been studied extensively throughout the last decades. Of particular note is the establishment of molar halogen-to-sulfur ratios, determined to be in the order of 0.3-0.7 for chlorine and 3×10^{-4} for bromine (e.g., Witt et al., 2008; Martin et al., 2010; de Moor et al., 2013). These halogen values are considered to be on the high end observed in magmas and plumes, yet are rather typical for arc volcanism (Aiuppa, 2009, Gutmann et al., 2018). Reactive bromine species (BrO) measurements were reported in the past (Bobrowski and Platt, 2007; Kern et al., 2009). Continuous composition monitoring (by Multi-GAS) has been realized since 2014 and gas data for the onset of the superficial lava lake was presented by Aiuppa et al. (2018).

In our field campaigns in 2016, UAV-based and ground-based sampling approaches were undertaken to study the plume of Masaya volcano with a focus on halogen emissions and atmospheric reactions of the emitted halogens. Samples were taken on the ground level at the edge of Santiago crater (Figure 1) at two locations (lookout south and pole site), at the top of the rim of Nindirí crater (Nindirí rim) and at Cerro Ventarrón. UAV-based sampling was conducted in the plume hovering over the Nindirí crater and above the caldera bottom and caldera rim (red points in Figure 1 (d)). Using ground based and UAV methods, the plume was sampled over a distance of about 2.8 km, covering an estimated age of 10 minutes, depending on the wind velocity.

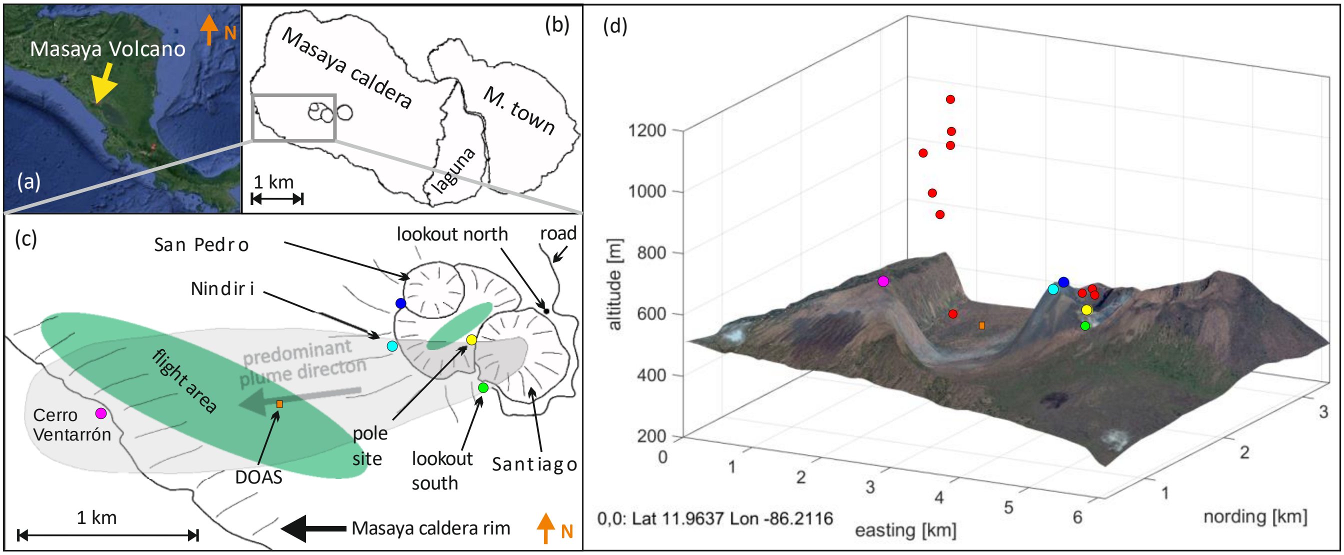

Figure 1: **(a)** location of Masaya volcano in Central America (© Google); **(b)** Masaya pit crater system in the Masaya caldera; **(c)** and **(d)** flight area (green patch and red points) and sampling locations marked by colored circles in sketched map and 3D plot.

3.2. Alkaline traps

Total halogen amounts were obtained by ground based sampling, using alkaline traps (Raschig tube (RT) and Drechsel bottle (DB)) (Liotta et al., 2012; Wittmer et al., 2014) at the locations marked in Figure 1. The alkaline solution quantitatively captures acidic gas species, due to an acid-base reaction, and enables the determination of total halogens (F, Cl, Br, I) and sulfur (S) concentrations. The sampled solutions were measured by ion chromatography (IC) and inductively coupled plasma mass spectrometry (ICP-MS) at the Geochemistry Laboratories of the Istituto Nazionale di Geofisica e Vulcanologia, Palermo (Italy). A 1 M NaOH solution was used in the RT and a 4 M NaOH solution was used in the DB. Both solutions were made from NaOH 99 % purity, Merck, Germany, in 18.2 MΩ cm^{-1} water. The plume samples were pumped through the RT using a GilAir Plus pump (Sensidyne, USA) for about one hour at 2.8 to 4 L min^{-1}. Total volume data logging enabled mixing ratio calculation of the RT samples. A custom-built pump (without data logging) was used to pump approx. 1 L min^{-1} of gas through the Drechsel bottles for between 18 and 30 hours each. These samples were used for gas ratio comparisons over a longer time period.

3.3. Gas diffusion denuder sampling

Reactive halogen species RHS were sampled by gas diffusion denuder samplers using 1,3,5-trimethoxybenzene as a reactive coating (Rüdiger et al., 2017) on borosilicate brown-glass tubes with a diameter of 0.9 cm. An electrophilic substitution reaction occurs within this coating, effectively trapping halogen species with an oxidation state (OS) of +1 or 0 (HalX, e.g., Br_2 (OS 0) or BrCl, BrNO3, BrO (OS +1)), which are considered as reactive species in contrast to the -1 OS species $Br^-_{(aq)}$ or $HBr_{(g)}$. However, it is not yet experimentally evidenced that the denuder technique is completely naïve to halogen radicals but following the chemical reaction mechanism the reaction of the denuder coating with halogen radicals is unlikely. Ground-based denuder measurements employed a serial setup of two denuders (2 x 50 cm) at a flow rate of 250 ml min^{-1} using a GilAir Plus pump and were conducted simultaneously to the RT sampling for 60 minutes to give the ratios of reactive species to total halogens (e.g., HalX/Br) or total sulfur (e.g., HalX/S). For the UAV based sampling, a remotely controlled sampler (called Black Box) was used, described in detail in Rüdiger et al. (2018). The typical sampling flow rate was about 180 ml min^{-1} for 5 to 15 minutes. The Black Box enabled logging of the sampling duration and SO_2 mixing ratios via the built-in SO_2 electrochemical sensor (CiTiceL 3MST/F, City Technology, Portsmouth, United Kingdom). Furthermore, the SO_2 sensor signal was transmitted to the remote control, which helped to identify regions of high SO_2 concentrations in real-time. The SO_2 signal of the sensor was time integrated over the sampling period of the denuders to derive the HalX/S ratios at the location where the UAV hovered during sampling.

3.4. Unoccupied aerial vehicle sampler

The UAV used for this study is a small four-rotor multicopter with foldable arms (Black Snapper, Globe Flight, Germany) called RAVEN (Rüdiger et al., 2018). We achieved flight times of up to 15 minutes with a payload of approximately 1 kg, depending on the sampling setup. GPS data of the flights was recorded onboard by using the micro-SD data logger (Core 2, Flytrex, Aviation, Tel Aviv, Israel) with a 2 Hz time resolution. The four batteries of the UAV were charged in the field with a car battery, enabling up to eight flights per day.

3.5. DOAS

DOAS measurements of SO_2 and BrO were performed by a scanning-DOAS station from the NOVAC network (Galle et al., 2010), which is located approximately 1.5 km WSW of Santiago crater at an altitude of 387 m a.s.l. (Aiuppa et al., 2018). This UV-spectrometer records the intensity spectra of the diffuse solar radiation over a wavelength range from 280-450 nm for different viewing angles by scanning the sky from horizon to horizon at steps of 3.6°. For most of the time, the volcanic plume transacts the scan plane nearly orthogonally. The slant column densities are retrieved from these spectra via the DOAS method (Platt and Stutz, 2008). Due to the rather high BrO detection limit, spectral and arithmetical averaging is required for a reliable retrieval of the BrO SCDs and ultimately the calculated BrO/SO_2 molar ratios. As a drawback, the temporal resolution of the BrO and BrO/SO_2 data is reduced to a data point roughly every 30 min. For a detailed methodological description see Lübcke et al. (2014) and Dinger (2019). Due to a data gap caused by an instrument outage, DOAS data for July 2016 was not available and therefore the times series only covers the later part of the field study. The obtained BrO/SO_2 ratios were investigated for a period between 06th of August 2016 and 30th of September 2016. The plume age was estimated by employing wind speed data obtained at the airport of Managua (Iowa State University, 2018), 18 km to the north of Masaya volcano. With an estimated plume height of 600 to 1000 m a.s.l. above the DOAS instrument (observed by UAV measurements) an estimation for the plume transition path length from the vent to the zenith position above the DOAS was calculated to be about 1.4 km. This distance was used to estimate plume ages for BrO/SO_2 ratios, by dividing 1.4 km by the wind speed obtained for the respective BrO/SO_2 ratios. These calculations resulted in plume ages between 1.4 and 11.1 minutes (see supplementary material Figure S1), which is reasonable compared to the estimated plume age for the UAV- and ground based data. There, an average plume age for the 2.8 km distance (*Cerro Ventarrón*) to the vent was estimated to be 9.3 minutes using a speed of 5 m/s. This wind speed was based on ground based measurements with a handheld anemometer taking during the field campaigns at the rims of Santiago and Nindirí craters. The wind speed measurements were performed during the ground-based sampling. It has to be stated that during the sampling procedures the wind speed was often unstable and the applied data is based on our spot check measurements and a source of uncertainty.

4. Modelling

In order to compare the results of the field measurements of RHS with theoretical predictions, the box model CAABA/MECCA (Sander et al., 2011) was used. In its base configuration, CAABA/MECCA simulates the chemistry of an atmospheric air parcel. In this study, however, it was adapted to the conditions of a volcanic plume with a focus on the chemistry of the bromine, chlorine and iodine. The atmospheric box model was initialized with the gas composition of the “effective source region” that was calculated by the thermodynamic equilibrium model HSC (HSC Roine A (2007) HSC chemistry 6.1. Tech. rep. Outotec Research Oy) and then quenched with ambient air to start the atmospheric model similar to earlier works (e.g., Gerlach, 2004; Bobrowski et al., 2007; Roberts et al., 2009; Roberts et al., 2014).

4.1. Thermodynamic equilibrium model (HSC)

Data from field measurements in 2016 determined the initial conditions for the model runs. SO_2, CO_2 and H_2O mixing ratios were derived from Multi-GAS measurements (de Moor et al. 2017; Rüdiger et al. 2018; Stix et al. 2018) and halogen amounts from the alkaline trap sampling. The sum of all gas mixing ratios were set to 100 percent to estimate the magmatic gas composition. H_2S and H_2 were not detectable (H_2S/SO_2 ratio < 0.01) by the Multi-GAS measurements and therefore neglected in the magmatic gas contribution. The high temperature magmatic gas composition was mixed with different percentages of ambient atmospheric background air resulting in different atmospheric-magmatic gas ratios (V_A:V_M), according to the calculations of Martin et al. (2006). The atmospheric background gas composition was taken from Roberts et al. (2014) (who used atmospheric background data for Etna volcano, Italy), since no detailed data on the atmospheric background composition at Masaya volcano was available, regarding trace gas species. The HSC model was reduced to produce gas species containing the elements (C, S, O, N, H, F, Cl, Br and I) and the temperature in the HSC model was arbitrarily set to 1000 °C. Similar to Roberts et al. (2009), this magmatic/ambient gas mixture of the “effective source region” was quenched with ambient air in order to obtain mixing ratios of all gas species (SO_2 mixing ratios are used as a proxy) for the initialization of the CAABA/MECCA model (Figure 2).

A list of the input and output species for the thermodynamic modelling of the high-temperature “effective source region” using the HSC model can be found in the supplementary material, as well as the atmospheric background composition (Table S 1).

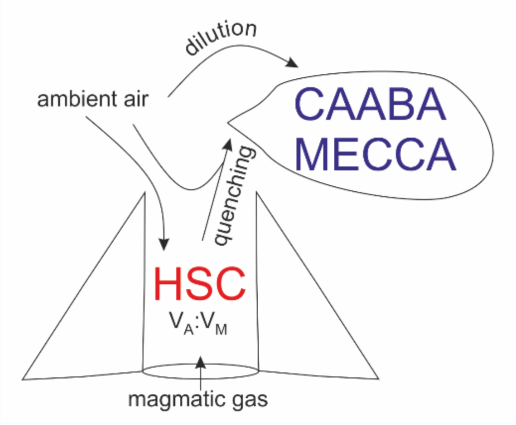

Figure 2: Sketch of the initialization process of the model.

4.2. Atmospheric box model (CAABA/MECCA)

The start point of the atmospheric chemistry box model was set to be within Santiago Crater, so the plume reaching the crater rim has already experienced chemical reactions. Thus, we were able to compare our field measurement results with the model output.

Throughout the box model run, further dilution with the same ambient air mixture was employed to entrain oxidants into the plume. In the box model, the dilution was achieved by adding an amount of ambient air, mixing it and then removing the same amount of mixed plume at a rate that achieves dilution to 1/e (0.37) over the dilution times listed in Table 2. For the dilution the composition of the ambient air was the same as in section 4.1 taken from Roberts et al. (2014). Aerosol data was taken from optical particle counter measurements at Masaya (Stix et al., 2018), which showed a bimodal distribution of particles with diameters of 1.1 and 2.4 µm and PM2.5 values reaching up to 5.4×10^3 µg m^{-3}. However, in CAABA/MECCA only a unimodal aerosol distribution was employed. The aerosol particle number concentrations and particle radii were varied in the model runs (see Table 2) to cover various particles masses and surfaces, including those observed in the field measurements. The aerosol chemical composition was set to be a 1:1 sulfuric acid / sulfate aerosol with ion concentrations according to the Köhler equation (Laaksonen et al., 1998) with given radii, temperature and relative humidity. Other parameters used in the CAABA/MECCA box model were a temperature of 298 K, a relative humidity of 80 % and a pressure of 960 hPa. The actinic flux was determined using the JVAL photolysis module (Sander et al., 2014) initialized for solar noon on 1 August at Masaya's latitude (11.98 deg N). The runtime of the model was 25 minutes with a time step of 2 seconds. With the initialization of the model, particulate sulfur accounts for less than 1 % of the total sulfur content. Comparison of the measurement data with the box model data was conducted by identifying model scenarios, which produce formation and progression of the bromine species and their ratios to total bromine and sulfur amounts comparable to what was measured. In order to simplify the selection of model scenarios that fit best with the observations, a computational procedure was chosen that compares the fit of model results for the progression of selected ratios (e.g. BrX/Br or BrO/SO_2) with the fit of the respective field measurements data (please see supplementary material for more details).

Two approaches were investigated: 1) molecular reactive bromine species BrX including Br_2, BrCl, $BrNO_2$, $BrNO_3$, HOBr, BrO) and 2) all reactive bromine species (r-Br), which also includes Br radicals (r-Br = BrX + Br radicals, see Table 2). The progressions of the respective reactive bromine species (BrX and r-Br) were fitted over the estimated plume age and the fit coefficients were compared with the coefficients from the field data to find the best agreement by minimizing the deviation of the respective fit parameters.

Table 2: Overview on chemical species abbreviations

BrX	Br_2, BrCl, $BrNO_2$, $BrNO_3$, HOBr, BrO
r-Br	BrX + Br radicals
Br	all Br species (measured by alkaline trap)
ClX	Cl_2, $ClNO_2$, $ClNO_3$, HOCl, ClO, OClO
r-Cl	ClX + Cl radicals
Cl	all Cl species (measured by alkaline trap)
IX	I_2, IO, INO_2, $IONO_2$, HOI, OIO, HIO_3, ICl, IBr
r-I	IX + I radicals
I	all I species (measured by alkaline trap)
NO_X	NO, NO_2
H_XO_Y	OH, H_2O_2, HO_2

Table 3: Thermodynamic (HSC) and box (CAABA/MECCA) model parameters, in bold measured parameters at the Santiago crater rim.

Parameter	Values		
HSC magmatic gas composition	Species	X/SO_2 (mol/mol)	Mixing ratio in the magmatic gas
	SO_2	**1.0**	0.015
	H_2O	**62.3**	0.93
	CO_2	**2.94**	0.044
	HF	**0.07**	1.05×10^{-3}
	HCl	**0.69**	1.03×10^{-2}
	HBr	**7.4×10^{-4}**	1.1×10^{-5}
	HI	**4.7×10^{-5}**	6.93×10^{-7}
HSC $V_A:V_M$	0:100, 2:98, 5:95, 10:90, 15:85, 35:65, 50:50		
Quenched SO_2 mixing ratios at model start	1000 ppmv, 500 ppmv, 300 ppmv, 30 ppmv, **6 ppmv**		
Reactive H_XO_Y, NO_X (NO, NO_2) species	HSC output (mag) or atmospheric background (air) (see Table S1)		
Dilution time to 1/e	10, 30, 60 minutes		
Aerosol number concentration	1×10^{8} m^{-3}, 1×10^{9} m^{-3}, 3×10^{9} m^{-3}, 5×10^{9} m^{-3}		
Aerosol particle size	50, 300, 900, 1500 nm		
Aerosol volume	5×10^{-14} to 9×10^{-8} m^3/m^3		
Aerosol surface	3×10^{-6} to 0.16 m^2/m^3 (**1.5×10^{-2} m^2/m^3**)		

5. Results and discussion

For samples taken on the ground e.g., at the crater rim of Santiago or on the rim of Nindirí the data includes denuder (reactive halogens e.g. Br_2, BrCl or in general BrX, ClX) and RT samples (total halogens e.g. total bromine (Br) chlorine (Cl)), while for aerial samples (e.g., caldera valley) RT data are not available. Ratios of the reactive halogens to sulfur or total halogen amounts were derived by employing the RT data and in the case of aerial samples data from the SO_2 electrochemical sensor. A comparison of a RT sample simultaneously taken to Multi-GAS measurements resulted in 4.18 ± 0.22 ppm of SO_2 in the RT sample and an average mixing ratio of 3.95 ± 0.20 ppm SO_2 for the Multi-GAS data. Based on Multi-GAS measurements conducted during the field campaign, which showed no presence of H_2S, it is assumed that the sulfur content of the alkaline trap samples originates mostly from SO_2. Particulate S could also be entrained by the alkaline trap, but is thought to contribute only a minor fraction of total S, as shown for Masaya by Martin et al. 2010 ($SO_2/SO_4^{2-} = 190$). Therefore, we regard the alkaline trap sulfur and the electrochemical sensed SO_2 as equivalent and use measured SO_2 mixing ratios as a plume dilution marker. The uncertainties of the obtained ratios are derived by the propagation of the errors of the analytical procedure and the sampling parameters. This includes the errors of GC-MS, IC and ICP-MS measurements as well as uncertainties in the sampling flow rate and the solution volume.

5.1. Total halogens

Sampling activities for a period of 9 days in July 2016 and 5 days in September 2016 gave 36 sample sets consisting of different combinations of alkaline traps, denuder and SO_2 sensor data (see Table S2). The alkaline trap samples were analyzed by IC and ICP-MS, whereas sulfur, fluorine and chlorine amounts were obtained by IC, bromine and iodine amounts were derived from ICP-MS analysis. The average molar (mol/mol) halogen to sulfur ratios (Hal/S) from samples taken at the crater rim are 0.07 ± 0.03 for fluorine, 0.69 ± 0.08 for chlorine, $7.4\times10^{-4} \pm 1.7\times10^{-4}$ for bromine and $4.6\times10^{-5} \pm 1.0\times10^{-5}$ for iodine respectively (see Table 4).

The halogen to sulfur ratios (Hal/S) obtained during the field campaign were categorized into groups with respect to their different sampling location, date and method (see Figure 3). For fluorine, bromine and iodine the deviation within the 4M NaOH solution samples (Drechsel samples) is larger than with chlorine. Whereas chlorine shows only a 6% deviation, deviations of 29% for I, 43% for Br and 62% for F are determined for the samples taken with DB. The 4M solutions were typically left at the site for overnight sampling (18-24 h). During this time, precipitation events might have affected the incorporated plume Hal/S ratios by different scavenging efficiencies for each halogen compound and water-solubilities of the respective gases. Duffel et al. (2003) also reported a high variability in HF data (obtained by Open-path Fourier transform infrared spectroscopy) and associated it to scavenging of the soluble HF by a condensed plume during overnight measurements. Different deposition rates of particulate and gas phases could cause loss of particles prior to sampling and therefore a larger variability in Hal/S ratios in overnight samples. Regarding the sampling location, on a first glance a difference in the Hal/S ratio can be noted between the crater rim and Nindirí rim. However, excluding samples that were taken under rather diluted plume conditions with a mean sulfur mixing ratio of < 1 ppmv, the difference in the Hal/S ratio between crater rim and Nindirí rim becomes negligible. While halogen and sulfur amounts in the considered samples were above the detection limit, one potential reason for discrepancies in the ratios may derive from contamination by entrained ash in the RT, although attention had been taken by pointing the RT- entrance away from the source. With lower overall plume enrichment in certain samples halogen-laden particle uptake could be a source for an increased Hal/S ratio in the Nindirí rim samples. A significant change in the I/S ratio between July and September is observable, which showed higher values in September, while the other Hal/S ratios do not change largely over this period (see supplementary material Figure S6). Using an average flux of 3029 ± 1396 t/day (1σ) of $SO_{2,}$ obtained by car DOAS traverses during the field work in July 2016 (de Moor et al. 2017) the following halogen fluxes were calculated for July 2016: 66 ± 40 t/day of HF, 1190 ± 130 t/day of HCl, 2.8 ± 0.7 t/day of HBr and 0.28 ± 0.06 t/day of HI. The cumulative error of the halogen fluxes is derived from the propagation of the SO_2 flux and the halogen to sulfur ratio uncertainties. The data set for halogens obtained in this study complements the measurements (filter packs) by Witt et al. (2008) in 2006 and Martin et al. (2010) in 2009 and is the first detailed data set on halogens for Masaya since the appearance of the lava lake (see Table 5). The Cl/S ratio is within the uncertainty of that reported by Martin et al. (2010) and twice as high as Witt et al. (2008). While the 2016 F/S ratio was about half of what was measured in 2009, the abundances of the heavier halogens have increased by a factor of ~2 for Br and ~3 for I compared to 2009, and are therefore significantly higher than the ratios in 2006 and 2009. Based on the CO_2/SO_2 ratio, Aiuppa et al. (2018) reported increased CO_2 emissions associated with the increased level and extension of the lava lake. For the period prior to the appearance of the lava lake the CO_2/SO_2 ratios were already higher than the reported ones for 2006 and 2009 and as well as the ones determined for the end of July 2016 until March 2017. Aiuppa et al. (2018) presented an average CO_2/SO_2 ratio of 5.5 ± 1.9 during the period of our measurements compared to 3.4 ± 0.5 in 2006 (Witt et al. 2008) and 2.7 ± 0.3 in 2009 (Martin et al. 2010) or 2.3–2.5 in 1998 (Burton et al., 2000). Alongside the halogen measurements in this study CO_2/SO_2 ratios were obtained in July 2016 (de Moor et al., 2017; Rüdiger et al., 2018) that represent rather short snapshot periods of few hours and resulted in values of 4.0 ± 0.6 and 3.6 ± 0.6, respectively, so lower than the average of Aiuppa et al., 2018. Compared to 2006 and 2009 the increased Br/S and I/S ratios in 2016 go along with observations of increased CO_2/SO_2 ratios (Table 5 and in Aiuppa et al. (2018)) while Cl/S ratios in 2016 are similar to 2009. Aiuppa et al. (2018) pointed out that the formation of the lava lake was associated with upward magma migration and deep rising CO_2-rich gas bubbles. Observations by Bobrowski et al. (2017) hinted on the potential increase of the ratio of heavier halogens to sulfur with higher CO_2/SO_2 ratios, on the other hand Cadoux et al. (2018) presented laboratory experiments with melts that indicate a contradicting behavior.

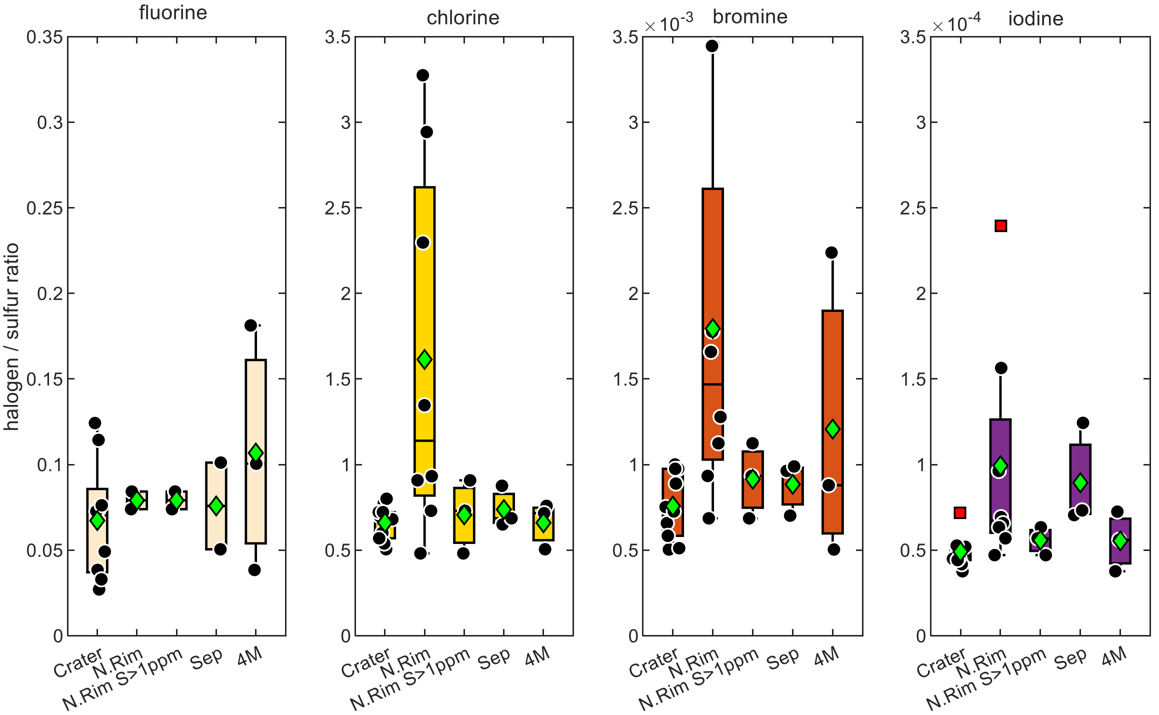

Figure 3: Evaluation of the measured halogen to sulfur ratios – Crater: Raschig tube in July at Santiago crater; N.Rim: RT in July at Nindirí rim; N.Rim S > 1ppmv: RT in July at Nindirí rim without samples with less than 1 ppmv sulfur; Sep: RT in September at Santiago crater; 4M: Drechsel bottle samples in July at Santiago crater with 4 molar NaOH solution; for each box, the black dots are the individual data

points, the central mark is the median, the green diamond is the mean, the box extends vertically between the 25th and 75th percentiles, the whiskers extend to the most extreme data that are not considered outliers, and the outliers are plotted individually marked by red squares.

Table 4: Median halogen to sulfur ratios measured at Santiago crater and downwind at Nindirí rim compared with downwind samples from a more dense plume S > 1 ppmv; the uncertainty is given as the median average deviation.

	F/S	Cl/S	Br/S	I/S
Crater	0.078 ± 0.028	0.69 ± 0.08	$(7.4 \pm 1.7) \times 10^{-4}$	$(4.6 \pm 1.0) \times 10^{-5}$
Nindirí Rim	0.079 ± 0.005	1.10 ± 0.53	$(15 \pm 4) \times 10^{-4}$	$(6.8 \pm 1.6) \times 10^{-5}$
Nindirí Rim, S > 1 ppmv	0.079 ± 0.005	0.73 ± 0.18	$(9.3 \pm 1.9) \times 10^{-4}$	$(5.7 \pm 6.5) \times 10^{-5}$
Crater September	0.076 ± 0.025	0.69 ± 0.04	$(9.6 \pm 0.3) \times 10^{-4}$	$(7.3 \pm 0.3) \times 10^{-5}$
Crater DB 4M	0.10 ± 0.06	0.72 ± 0.04	$(8.8 \pm 3.8) \times 10^{-4}$	$(5.6 \pm 1.6) \times 10^{-5}$

Table 5: Halogen to sulfur and inter-halogen ratios of Masaya's gas emissions between 2006 and 2016.

	Witt et al. 2008	Martin et al. 2010	this study
year	2006	2009	2016
F/S	n.d.	0.13 ± 0.01	0.07 ± 0.03
Cl/S	0.32 ± 0.01	0.77 ± 0.06	0.69 ± 0.07
Br/S	$(2.7 \pm 0.2) \times 10^{-4}$	$(3.2 \pm 1.0) \times 10^{-4}$	$(7.4 \pm 1.7) \times 10^{-4}$
I/S	$(1.8 \pm 0.1) \times 10^{-5}$	$(1.5 \pm 0.2) \times 10^{-5}$	$(4.6 \pm 1.0) \times 10^{-5}$
Cl/F	n.d.	6.0 ± 0.3	9.9 ± 4.1
Cl/Br	$(1.2 \pm 0.1) \times 10^{3}$	$(2.4 \pm 0.7) \times 10^{3}$	$(0.9 \pm 0.2) \times 10^{3}$
Cl/I	$(1.8 \pm 0.1) \times 10^{4}$	$(5.0 \pm 0.4) \times 10^{4}$	$(1.5 \pm 0.4) \times 10^{4}$
CO_2/SO_2 [a]	3.4 ± 0.5	2.7 ± 0.3 [#]	4.0 ± 0.6 [b] and 3.6 ± 0.6 [c] [*]

Halogen data from Witt et al. and Martin et al. was derived from filter pack measurements; [a] Multi-GAS (MG) data; [b] MG data from (de Moor et al., 2017); [c] MG data from (Rüdiger et al., 2018); # OP-FTIR data

5.2. Reactive halogens

Reactive halogens were measured by gas diffusion denuder sampling. The reactive halogen data are categorized by their sampling location and the median of the species ratios for each location was calculated together with their propagated uncertainties (Table 6). For each location, a distance to the vent was estimated based on path of the downwind drifting plume and GPS data of the sampling locations. For aerial samples the GPS coordinates of the highest measured SO_2 mixing ratios were chosen as a representative location. The uncertainties of the distance were estimated for each location based on the spatial distribution of the respective samples. Figure 4 shows the reactive halogen to sulfur (HalX/S) and reactive halogen to total halogen (HalX/Hal) ratios as a function of the distance to the vent. For bromine, whose activation in volcanic plumes has been studied extensively in the past (e.g., Oppenheimer et al., 2006; Bobrowski et al., 2007; Bobrowski and Platt, 2007; Bobrowski and Giuffrida, 2012), an increase of the BrX/S and BrX/Br over distance and therefore plume age is clearly observable. The ratio of BrX/S increases from (1.3 ± 0.6) $\times 10^{-4}$ at the crater rim up to (20 ± 14) $\times 10^{-4}$ downwind location above the caldera valley (red dots in Figure 1). Also, the BrX/Br ratio increases from 0.20 ± 0.13 at the crater rim to 0.76 ± 0.26 at *Cerro Ventarrón* (purple dot). Those ratios obtained for the crater rim are in the range of what was recently measured at the volcanoes Etna (Rüdiger et al., 2017), Nyamulagira (Bobrowski et al., 2017) and Stromboli (Rüdiger et al., 2018) by the same method and at similar distances from the vents. Although the Br/S ratio increased from 2009 to 2016 the average BrO/SO_2 ratio from August to September 2016, 3.4 $\times 10^{-5}$, is similar to observations by Kern et al. (2009) (average of 3.0×10^{-5}) who conducted measurements at the crater rim of Santiago crater in 2007. However, measurements of BrO/SO_2 ratios in 2003 had been significantly lower with about 1.1 $x10^{-5}$ (Platt and Bobrowski, 2015).

Due to technical problems causing instrument outage, DOAS data were only available for the period shortly after the field campaign in July 2016, but we assume that no significant changes in the degassing behavior occurred between July and September 2016, which is plausible regarding the stable CO_2/SO_2 gas ratios presented by Aiuppa et al. (2018) for that period. Therefore, a comparison of the BrO/SO_2 and BrX/S ratios is feasible. For the plume measured by the DOAS instrument in the zenith orientation, we estimated a distance to the vent of 1.4 km and employed wind speed data to derive an estimated plume age, which is presented in Table 7. By using those data BrO accounts for approximately 10 % of the reactive bromine species for plume ages (< 5 min.) (see Figure 5). The apparent increase in the BrX/S ratio after 6 minutes needs to be regarded with caution, since the downwind BrX/S ratio was obtained in a diluted plume, which is a source of uncertainty, due to low SO_2 mixing ratios. The denuder sampling enriches reactive species on the coating and therefore achieves a better detection limit with time. The electrochemical sensor signal on the other hand, is limited by the instrumental detection limit and time-integrated SO_2 mixing ratios may not include phases in which SO_2 was present but below the limit of detection (0.1 ppmv). Therefore, SO_2 might be underestimated and the BrX/S ratio might be overestimated in the diluted plume. These uncertainties are included in the error estimation giving by the error bars of this respective sample. The farthest downwind BrX/S ratio was obtained by a calculation that employs the BrX/Br ratio and the total Br/S ratio, due to sulfur being below detection limit with the IC method. The propagation of the respective uncertainty is included in the error bars as well. However, since the uncertainties are known and estimated, the resulting BrX/S progression still provides insights into the chemistry of the plume. The comparison with the BrO/SO_2 ratios underlines the postulated reaction mechanism, in which BrO is an intermediate product that further reacts to form other reactive species as shown by the reaction paths in Table 1. Therefore, BrO might reach a rather steady state of being formed and reacting to other compounds (e.g., Bobrowski and Giuffrida, 2012; Gutmann et al., 2018).

Furthermore, an activation of chlorine was observed, which has also been detected in the past by remote sensing techniques at other volcanoes but not at Masaya (e.g., Lee et al., 2005 (Sakurajima); Bobrowski et al., 2007 (Etna); Donovan et al., 2014 (Sourfirere Hills); Gliß et al., 2015 (Etna)). Regarding reactive chlorine ClX (Cl_2, $ClNO_2$, $ClNO_3$, HOCl, ClO, OClO) both the

ClX/S and the ClX/Cl ratio increase with distance from the vent. While bromine is activated largely, chlorine activation is only observed in the order of 10^{-4} of total chlorine. Due to the higher total chlorine abundance ClX, mixing ratios still show similar values as BrX. Roberts (2018) pointed out that the significant Cl activation would only occur if HBr has already been transformed to BrX and therefore the reaction channels R4b, R5b, R6 and R8 would play a more important role, which lead to the activation of via BrCl and Cl radicals to form ClO with ozone and OClO from ClO and BrO. Recently, Kern and Lyons (2018) observed a lack of OClO in the center of a volcanic plume by DOAS measurements, while it was increased (relative to SO_2) at the edges. They attributed this observation to the incomplete activation of Br in the plume center and dominance of Br_2 formation (R4a) over BrCl formation (R4b) with an undepleted reservoir of particulate Br. However, Kern et al. (2009) did not detect ClO or OClO in the plume of Masaya close to the vent, but presented a detection limit for ClO/SO_2 and $OClO/SO_2$ of 5×10^{-3} and 7×10^{-6}, respectively. Since the ClX/S ratios potentially include ClO and OClO as reactive chlorine species, we applied a calculation shown in Kern et al. (2009) (equation 2) to compare our results with their detection limit (for long path DOAS). Under the assumption that ClX is made up by only ClO and no OClO, and BrO is 10% of the measured BrX at the crater rim, a potential $OClO/SO_2$ ratio of 3.5×10^{-5} was calculated by employing the rate constant and photolysis frequency for the formation and depletion of OClO at an average SO_2 mixing ratio of 6 ppmv at the crater rim measurement site. The calculated $OClO/SO_2$ ratio is above the estimated detection limit for OClO by Kern et al. (2009) by a factor of 5. With ClO accounting for 20 % of ClX, which is a high estimate according to the model run presented in section 5.4.3 and Figure 9, the $OClO/SO_2$ ratio (7×10^{-6}) would be in agreement with the DOAS measurements conducted in 2007 by Kern et al. (2009).

Since iodine is the least abundant halogen in volcanic gases, it has not been observed in many previous studies. The detection of reactive iodine in volcanic plumes was limited to one satellite based study of IO (Schönhardt et al., 2017) in the plume of Mt. Kasatochi in 2008. Due to its low abundance, it is challenging to determine iodine in alkaline trap samples as well as in denuder samples. The ratios of activated iodine to activated bromine (0.16 at Santiago crater, 0.12 further downwind) are in the same order of what Schönhardt et al. (2017) presented for the IO/BrO (0.09), and iodine activation shows a similar trend as bromine (Figure 4). The IX/I ratio increases from 0.3 close to the emission source to 0.9 about 10 minutes downwind, while the IX/S ratio increases by a factor of 5 to 10 on the same distance (Table 6).

5.3. Nighttime sample anomaly

One simultaneous denuder and RT sample was taken during a nighttime visit at the crater rim in 2016 (sampling duration approx. 1 hour). This sample shows an anomalous value for reactive chlorine (see Figure 4). The values for reactive bromine and iodine are similar to that one measured at the same location during the day. One possibility is that this value is an artifact caused during sampling or analysis. However, the absolute signal of Cl-TMB on the respective denuder was above the average signal produced by the highest concentrated calibration standard. Therefore, a contamination by a calibration standard during the analysis can be ruled out. Since the sample was measured in triplicate, a random instrument error is also unlikely. A potential contamination during the sampling in the field or in the laboratory by a different chemical compound would have needed to produce the same retention time and m/z ratio as Cl-TMB, which we assume to be unlikely.

A potential explanation for this high reactive chlorine value is the enhancement of chlorine species at night that are otherwise photolyzed at daytime. A fraction of the HalX species is already formed by high-temperature reactions on the surface of the lava lake (e.g., Br_2, Cl_2) (Martin et al., 2006) and can be measured at the crater rim without involving photochemistry. For example, the HSC equilibrium model (see section 4.1) for bromine speciation at 1000°C gives a Br_2/HBr ratio of 10^{-4} for an air entrainment into plume gas of 2-5%, which is in the range of the nighttime sample. Regarding reactive chlorine, the HSC model predicts a substantial fraction of Cl atoms (0.1 % of HCl). The Cl atoms can react with each other to form Cl_2 by recombination (Hippler and Troe, 1976), which is more than two orders of magnitudes faster than the reaction of Cl with methane (Bryukov et al., 2002). Therefore, a formation of Cl_2 in the cooled plume gas mixture, after the emission at the lava lake surface and prior to sampling at the crater rim, would induce a larger night time signal compared to the day with photolysis happening under the assumption that elemental chlorine is not trapped by the currently used denuder coating (Rüdiger et al. 2017).

Table 6: RHS to sulfur and total halogen ratios at five different locations and estimated plume ages at 5 m/s wind speed, median values, bdl = below detection limit

location ground / air	distance [m]	age [min]	chlorine		bromine		iodine	
			ClX/S ×10^{-4}	ClX/Cl ×10^{-4}	BrX/S ×10^{-4}	BrX/Br	IX/S ×10^{-5}	IX/I
Santiago rim (g)	217±20	0.7	2.1 ± 0.4	2.7 ± 0.7	1.3 ± 0.6	0.20 ± 0.13	2.1 ± 0.9	0.32 ± 0.15
Nindirí crater (a)	342±50	1.1	3.3 ± 1.0		3.0 ± 0.1		1.1 ± 0.1	
Nindirí rim (g)	737±50	2.5	16 ± 9	11 ± 3	5.0 ± 3.4	0.67 ± 0.05	3.9 ± 1.4	0.31 ± 0.14
Caldera valley (a)	2002±100	6.7	bdl		20 ± 14		11 ± 1	
Cerro Ventarrón (g)	2800±200	9.3	bdl	bdl		0.76 ± 0.26		0.92 ± 0.67

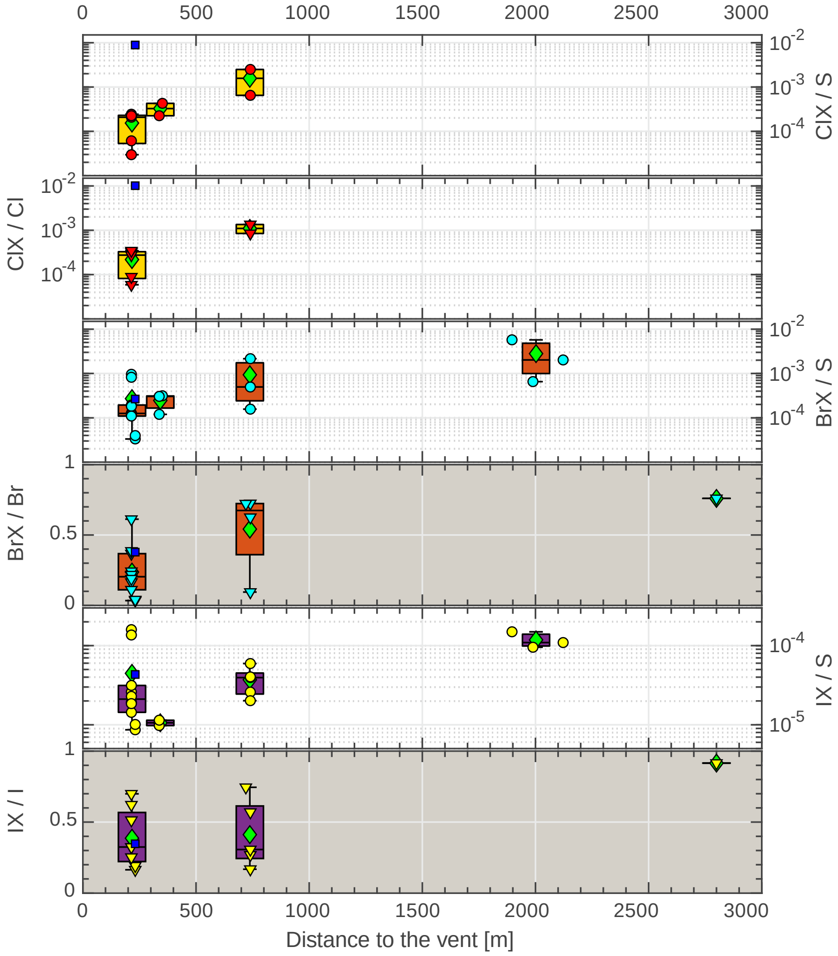

Figure 4: RHS progression during plume aging, note the non-logarithmic scale with the gray background; circle: Hal/S; triangle: HalX/Hal; diamond: mean; box plot: 25 & 75 percentile and median; blue square: night sample (not included in mean and median calculation).

Table 7: BrO/SO₂ ratios from a stationary NOVAC DOAS instrument at the estimated plume ages obtained from wind speed (see section 5 3.5 and supplementary material Figure S2, the values marked with * are single data points with the uncertainty of the single measurement, the other uncertainties derive from multiple measurements and the respective standard deviation).

estimated plume age [min]	average BrO/SO$_2$ ratio ×10^{-5}
1.4	0.95 ± 1.06*
2.2	3.69 ± 1.05*
3.2	2.87 ± 0.31
3.7	2.95 ± 0.56
4.4	2.53 ± 0.75
5.5	2.72 ± 0.83
7.4	3.18 ± 0.83
11.1	3.68 ± 1.22

Table 8: H_XO_Y and NO_X species used for the initialization of the CAABA/MECCA model runs.

	OH	**H_2O_2**	**HO_2**	**NO**	**NO_2**
air	7×10^{-13}	0	3×10^{-11}	5×10^{-11}	1×10^{-10}
mag (5:95)	4×10^{-9}	1×10^{-12}	4×10^{-11}	3×10^{-9}	1×10^{-10}
mag (10:90)	5×10^{-9}	2×10^{-12}	4×10^{-11}	8×10^{-9}	1×10^{-10}

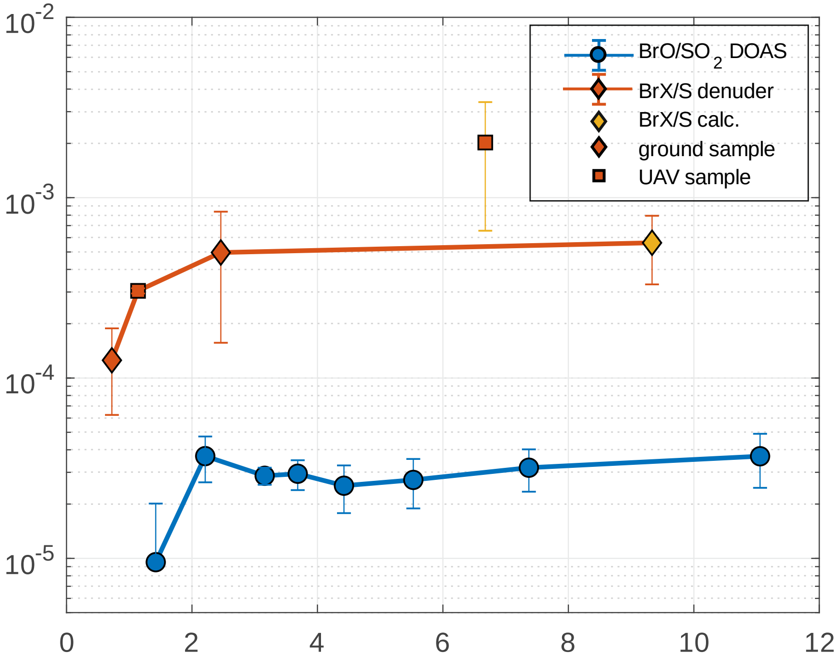

Figure 5: Average RHS/S ratios with plume age: BrO/SO_2 ratios measured by a stationary DOAS instrument and BrX/S ratios obtained by ground- and aerial-based denuder sampling; BrX/S calculated value derived by from BrX/Br ratio at this plume age and crater rim Br/S value. The UAV sample could be affected by underestimation of SO_2 (see text).

5.4. Comparison with box model results

A two-stage chemistry modelling approach (see section 4) was applied to analyze the field observations. The two major objectives are: (1) investigating the field data for plausibility, and (2) applying the CAABA/MECCA box model in the field of volcanic plume chemistry. The output of the HSC model gives 110 gas species of which 42 were used as input for the CAABA/MECCA box model, that are listed in the supplement material Table S1 (including also the halogen radicals). By iterating the various parameters for the model start condition that are shown in Table 3, 3816 different model runs of were performed. Each model run simulated the progression of the set of model species during the first 25 minutes. As reactive bromine species are the best studied reactive halogens in volcanic plumes, this section is mostly focused on Br. The measurement data (denuder) give the sum of reactive bromine species and the model data provide detailed speciation information. The comparison was conducted by a script-based routine, which was required to evaluate the large number of model runs. The routine compares the fit parameters of the progression of the measurement data with the respective model speciation output for bromine (see section 4.2 and supplementary Figure S2). Several ensembles of start parameters match the measurement data in good agreement. Although the progression of BrX/Br and r-Br/Br deviate in certain model runs quite substantially, only the BrX/Br progressions are discussed in more detail for the sake of clarity. Please see the supplementary material for more details on r-Br/Br progressions.

5.4.1. Bromine chemistry

For the BrX/Br progression, the best matching scenarios are presented in Figure 6 (dashed lines). Furthermore, the BrO/SO_2 progressions were also fitted separately and the best matching model runs with regards to BrO/SO_2 are presented as well (dotted lines). In Figure 6, the solid lines represent those model runs, which show the smallest deviation between the measured data and modelled data for both BrX/Br and BrO/SO_2 ratios.

BrX/Br progressions

Figure 6 shows the progression of the bromine species over the model time of 25 minutes and the corresponding field measurements. The best matching model scenarios imply atmospheric gas to magmatic gas ratios V_A:V_M of 15:85 or less. Roberts et al. (2014) considered a V_A:V_M of 10:90 or less as likely for system like Etna volcano. For Masaya volcano with its active lava lake, we consider V_A:V_M of up to 15:85 as realistic with respect to the potentially stronger mixing of atmospheric and magmatic gases at the lava lake-atmosphere interface. Besides the initial halogen speciation, changes in V_A:V_M also affect the initial H_XO_Y/NO_X mixing ratios (see Table 8). The model runs were either conducted with the H_XO_Y/NO_X mixing ratios produced by the HSC model (magmatic scenario: more H_XO_Y/NO_X) or the respective atmospheric background mixing ratios atmospheric scenario: less H_XO_Y/NO_X) at the model initialization. Therefore, best matching model runs are both shown for initial magmatic (red lines) and atmospheric (blue lines) H_XO_Y/NO_X scenarios in Figure 6. Roberts et al. (2014) already discussed the discrepancy between a kinetically limited formation of NO_X from background N_2 and the contradicting observations of H_XO_Y/NO_X compounds at the crater rim (e.g., Oppenheimer et al., 2010; Carn et al., 2011; Martin et al., 2012). The HSC model might over predict NO_X since its formation is kinetically limited as a result of the high bond strength of N_2 that is entrained in the plume. Roberts et al. (2014) alluded the need for an alternative explanation for NO_X at volcanoes, where it has been observed. In a recent study Roberts et al. (2019) presented a time-resolved chemical kinetics model for the high temperature near source chemistry of volcanic emissions that is an improvement to the HSC model. In contrast to HSC, Roberts et al. (2019) reproduced reduced gas species and high temperature formation of HO_2, OH, and H_2O_2, but do not include NO_X chemistry yet. Therefore, two scenarios with magmatic and atmospheric H_XO_Y/NO_X composition are investigated as extremes, representing the HSC output and the atmospheric background composition, respectively. It has to be noted that the chemical compositions of these two scenarios represent actual extremes rather than reality, which should be somewhere in between. Since the HSC output is biased by the limitations of the model (see section 2) and the choices of the used initialization parameters and the atmospheric background composition at Masaya volcano (boundary layer) might be different than the one used in this study taken from Roberts et al. 2014 for Etna volcano (free troposphere).

BrX/S progressions

For the progressions of BrX/Br as well as BrO/SO_2 ratios, model scenarios with a good agreement to the measurement data have been identified. However, for the BrX/S ratios (Figure 6b) the model underpredicts the field observations. In the modelled BrX/S ratios S represents the total sulfur content (all S species), which is constant, except for dilution. The prediction of the BrX/Br progressions are in better agreement with the measured data. As above mentioned (section 5.2) we think that the measured BrX/S ratios could be overestimated due to underestimation of SO_2, especially in the samples obtained by UAV measurements, which can be explained as follows. An underestimation of sulfur could be the case when the plume is diluted and SO_2 is below the detection limit of electrochemical sensor. Under these circumstances, the sensor does not detect SO_2 while the denuder is still trapping small amounts of reactive Br, resulting in an overestimated BrX/S ratio. Other hypotheses addressing the discrepancy in observed and measured BrX/S progressions could be related to the heterogeneity of the actual plume caused by “puffs” with high and low concentrations and therefore different chemistry compared to the modelled “bulk plume” or different background ozone (NO_X, HO_X) levels than assumed for this study.

BrO/SO_2 progressions

The measured BrO/SO_2 progression (Figure 6c) could be reproduced by various model runs with different $V_A:V_M$ ratios, H_XO_Y/NO_X mixing ratios and initial start concentrations. The BrO/SO_2 ratio is only slightly over predicted in the model runs that fitted best for the BrX/Br progression. This overprediction is smaller for the model run with the magmatic H_XO_Y/NO_X scenario (see Table 8). Potentially, a higher abundance of H_XO_Y and NO_X species could promote the loss of BrO to form HOBr and $BrNO_3$. The model runs that show a good agreement with the BrO/SO_2 progression (Figures 6c) are able to reproduce the fraction of BrO of the total reactive bromine (5-15 %) (Figure 6d) comparable to what was observed in the field data (~10 %). Employing a conversion of total Br to reactive Br of 67 % for a plume age of 2.5 minutes (Table 6) and a BrO fraction on the BrX of 10 %, BrO accounts in our case for roughly 7 % of the total bromine. Recently Gutmann et al. (2018) compiled data on the extent of the BrO/Br fraction at Masaya and presented values of 5-15 % increasing with the distance to the crater.

Detailed bromine speciation

Figure 7 gives an overview on the detailed bromine speciation during the first 25 minutes of the model runs that were fitted best to the observations of the reactive bromine progressions and the BrO/SO_2 data. For both approaches with and without including Br radicals to the species measured by the denuders one atmospheric and one magmatic scenarios is presented in detail. It is noticeable that the BrCl fraction is more elevated in the scenarios with a magmatic H_XO_Y/NO_X composition compared to the atmospheric scenarios, while the Br is less prominent. BrCl is photolyzed slower than Br_2 (Maric et al., 1994), therefore a larger fraction of BrCl, compared to Br_2, could cause a slower formation of Br. The BrCl fractions might also be enhanced due to larger abundances of ClX, including ClO, OClO and Cl_2.

In all four runs of Figure 7, the HBr mixing ratios decrease rapidly after initialization as it is transformed to reactive species or taken up by the aerosol. Less aerosol (particle number concentration and diameter) leads to a slower loss of HBr (Figure 7a). Only a small amount of bromine is present as aqueous $Br^-_{(aq)}$. Regarding the heterogeneous reaction mechanism of the "bromine explosion", aqueous $Br^-_{(aq)}$ and $HOBr_{(aq)}$ is needed to form Br_2, which is then emitted from the particle. As the modeled outgassing of Br_2 is faster than the uptake of HBr and HOBr, bromide is depleted from the particles. At low levels of aerosol bromide, reaction (R4b) produces BrCl and represents another sink for HOBr. Formation of BrCl by the mentioned reaction (R4b) is also known for other systems e.g., simulated ice surfaces (e.g., Fickert et al., 1999; Huff and Abbatt, 2000).

Comparison with other volcanic plume modelling

We compared our model study to earlier studies that applied the models MISTRA (von Glasow, 2010) and PlumeChem (Roberts et al., 2014), which were based on volcanic plume measurements at Mt. Etna. All three studies succeed to simulate a bromine activation to the magnitude measured by our denuder sampling technique. However, the differences in the specific species making up reactive bromine is substantial. While similar to our results, PlumeChem reproduces a large fraction of Br_2 as well as a local maximum in the young plume (~ 5 min), MISTRA on the other hand shows a constant fraction of approximately 5-10 %. The modelled HOBr in PlumeChem is also in agreement for the first 10 minutes with our CAABA/MECCA output. But regarding BrO, our finding is comparable to results of MISTRA which produces less than 10 % BrO of the total Br in the young plume, while PlumeChem models a varying BrO fraction between 10 % and 50 % of the total Br, depending on the initial total Br/S ratio and BrO reaching a fraction of ~ 50 % of the reactive bromine in all its scenarios. Furthermore, the substantial contribution of BrCl, which we simulated was not presented by MISTRA or PlumeChem. $BrNO_3$ (formed by BrO and NO_2) on the other hand is present in PlumeChem and CAABA/MECCA, while MISTRA produces $BrNO_2$ as a reactive bromine-nitrous species. In our model run in Figure 7b the fraction of $BrNO_3$ is larger compared to the other scenarios, although in the magmatic scenario NO_2 mixing ratios are similar to the atmospheric background. But in the case of Figure 7b, NO is more abundant and can form NO_2 under O_3 consumption to react with BrO to $BrNO_3$. However, the formation of $BrNO_3$ is limited by the photo-labile NO_2 and also a competitive reaction of BrO with HO_2, ClO, and itself (R 2a, 2b, 6, 8). In order to explore the reason for those model differences in more detail, the reaction mechanisms used by the three models need to be compared and similarities and differences in reaction rates shall be evaluated. This however lies beyond the objectives of this work.

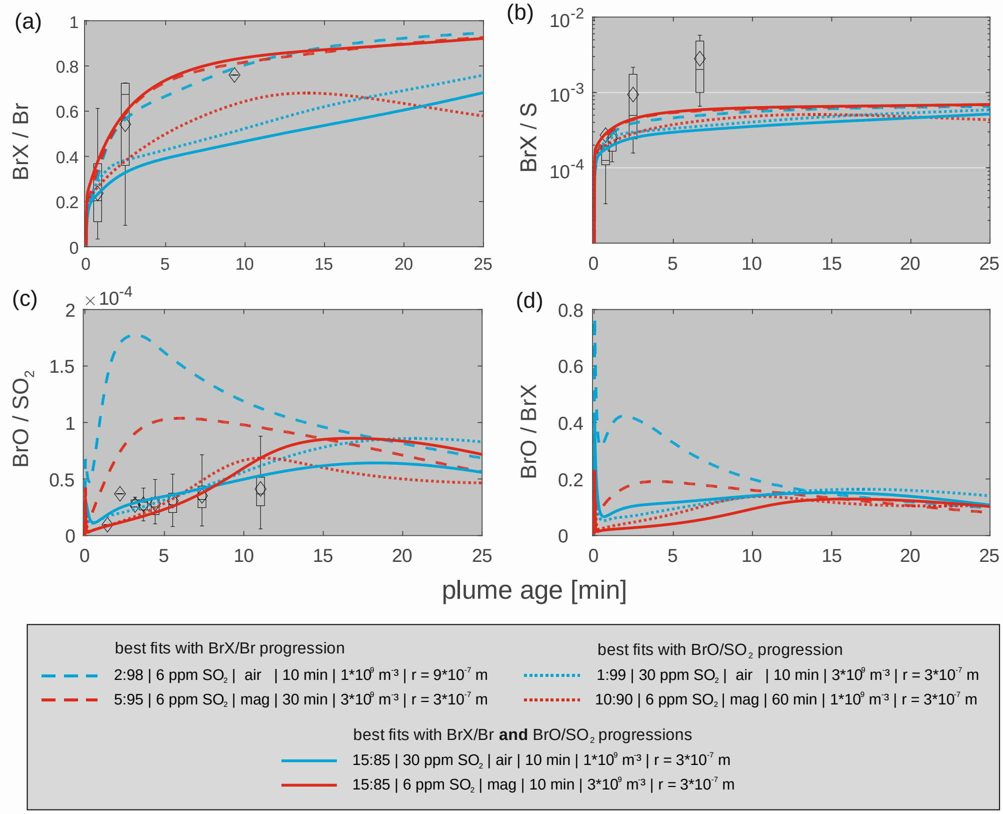

Figure 6: Temporal evolution of different modelled bromine species ratios (molar) over the model time of 25 minutes with the respective measurement data (if available). Each sub figure shows the model runs that are closest to the measurement data, derived by the fit comparison

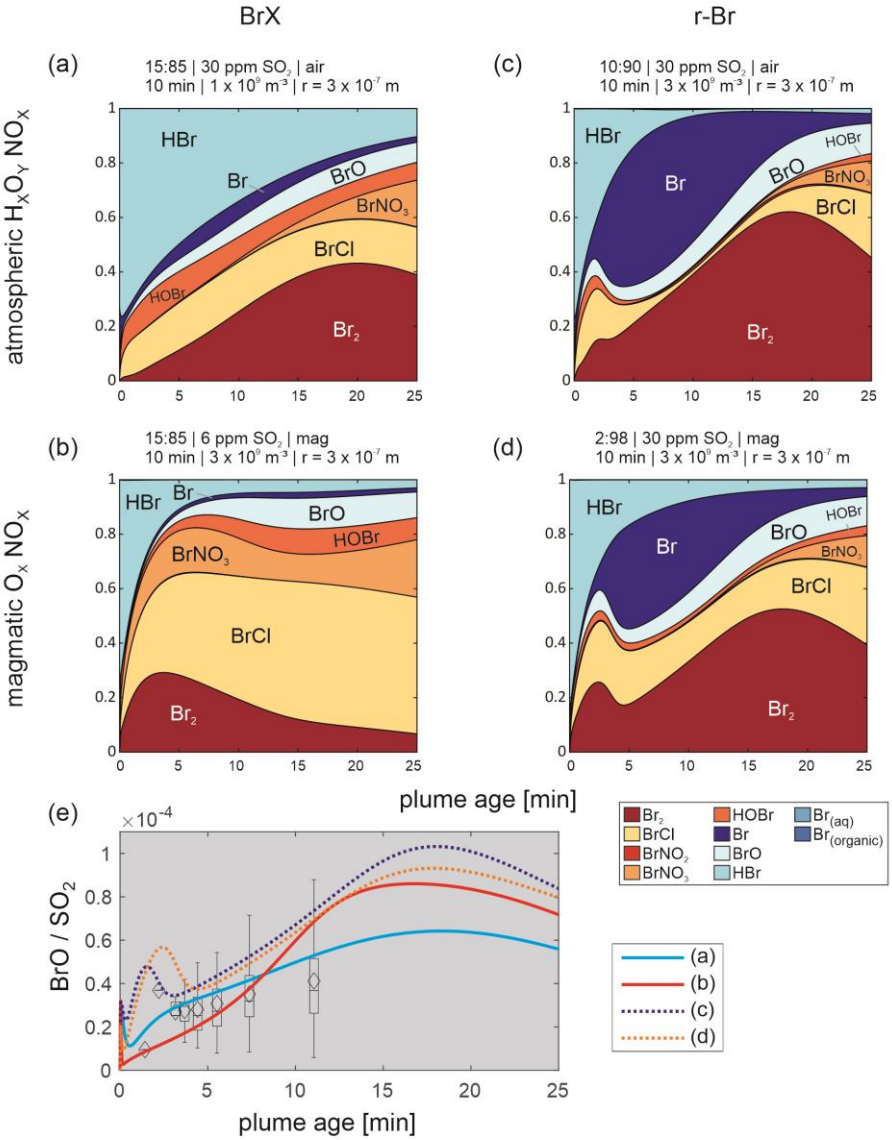

Figure 7: (a-d) Detailed bromine speciation for the first 25 minutes of four selected model runs closest to the measured BrX/Br, r-Br/Br and BrO/SO$_2$ progressions . Four different model scenarios are shown, that fit best to the measurement data, using the progressions of BrX/Br and r-Br/Br with magmatic and ambient air oxidants amounts respectively; **(e)** the corresponding BrO/SO$_2$ ratios to the model runs of (a-d).

5.4.2. Input parameter sensitivity analysis

The so-called base run of CAABA/MECCA box model, which encompasses the set of parameters from Table 3 that produced the most proximal model recreation to the field observations of the BrX/Br was chosen to study sensitivity of the model with regards on changes of initial start conditions. These start conditions are:

(1) the initial volume ratio of atmospheric gas to magmatic gas (V_A:V_M)

(2) the quenching factor (QF) for the initial quenching of the mixture of high-temperature gases to low temperature conditions with ambient air (e.g., quenching to 6 ppmv SO_2)

(3) the dilution time (τ) of the plume, within the initial mixing ratio of an inert species gets diluted by a factor of 1/e (0.37).

(4) the quantity of reactive oxidants H_XO_Y and NO_X

(5) the number concentration (NC) of particles per m³

(6) the radii of the particles

The model run shown in Figure 7c was chosen as the model base run. This is based on two considerations. First, an atmospheric H_XO_Y/NO_X scenario is more likely than a magmatic scenario due to the kinetically limited formation of NO_X species by high temperature chemistry in the "effective source region". Secondly, even though the potential measurement of Br radicals by the denuder technique cannot be ruled out, the discrepancy between the progressions with and without Br radicals in Figure 7c is still within the deviation of the measurement data. Therefore, the base run (best fit in Figure 7 with the r-Br/Br progression (10:90 | 30 ppmv SO_2 | air | 10 min | 3×10^9 part. m^{-3} | $r = 3\times10^{-7}$)) was used with permuted start conditions to evaluate the influence of these conditions on the specific model outcome. The results of these tests are shown in Figure 8.

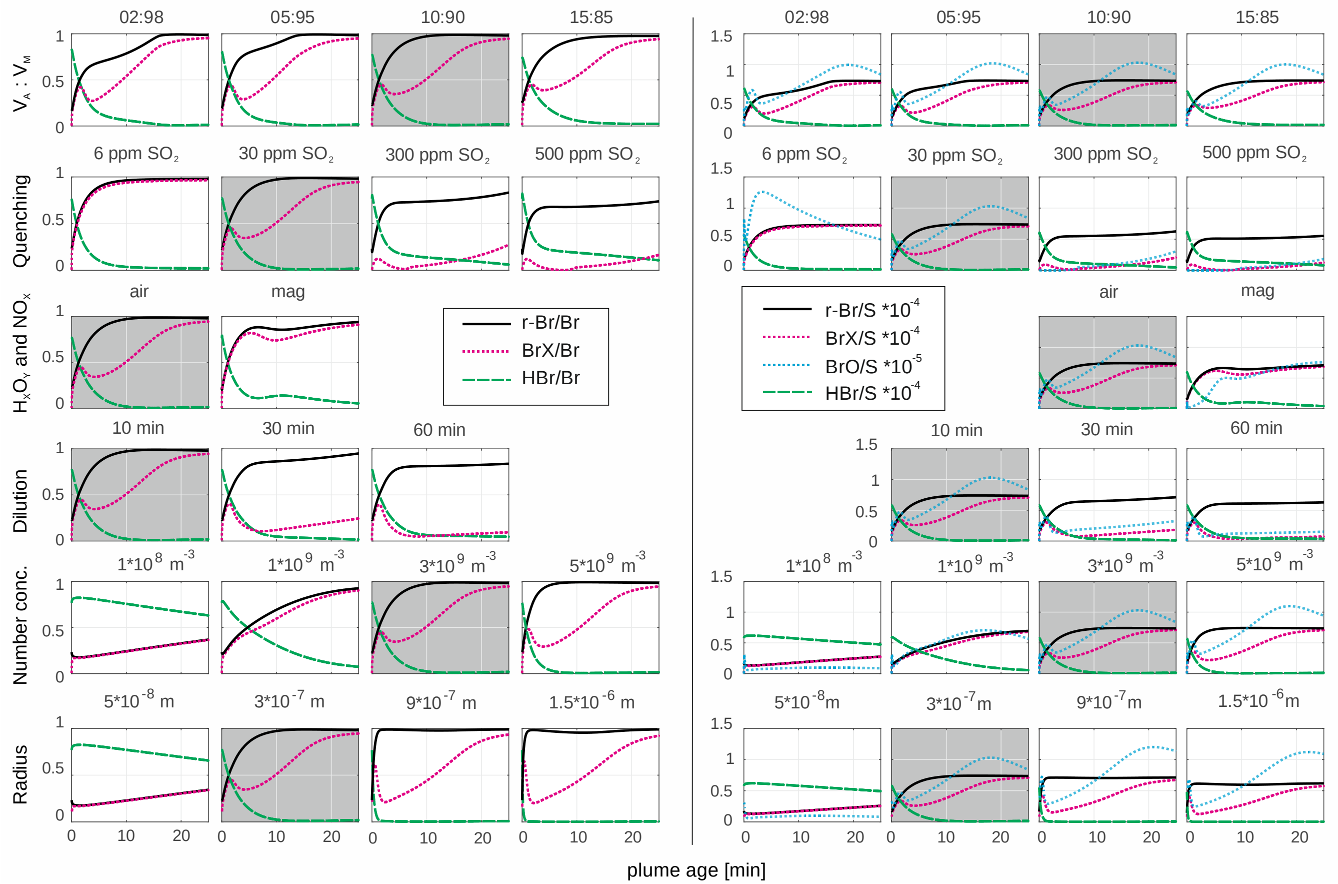

Figure 8: Progression of selected bromine species over a model runtime of 25 minutes related to total bromine (left half) and sulfur (right half) abundances. The best fit to the measurement data from Figure 7 (c) (10:90 | 30 ppmv SO_2 | air | 10 min | 3×10^9 part. m^{-3} | r = 3×10^{-7} m) is shown with gray background and within the specific rows the one model parameter is varied over different values in order to explore the model output answer to the model input change.

Changes in the initial V_A:V_M ratio (in the case of $V_M \geq 85$ %) has only little effect on the BrX/Br or BrX/S ratios, while r-Br/Br is slightly smaller for $V_M \geq 95$ %. There, potentially less Br radical is formed with less atmospheric gas in the HSC model. The QF shows a significant impact, in the base run a quenching to 30 ppmv SO_2 reduces the presence of Br radicals and almost equals r-Br and BrX. Less quenching, indicated by higher SO_2 mixing ratios, leads to less r-Br formation (relative to total Br) and increases the fraction of Br radicals. The relative BrO abundance is also reduced with less quenching due to the larger abundance of bromine in the modelled scenario, while the O_3 entrainment stays fixed. Therefore, more Br is available to consume the same amount of O_3, resulting in less relative formation of BrX. Likewise, a slower dilution results in slower in-mixing of O_3 into the plume causing slower formation of BrX and BrO. The shape of the BrX species progression in the scenarios with less quenching (30 to 500 ppmv SO_2) and slower dilution time (30 and 60 minutes) are related to a substantial consumption of ozone in the modelled plume (see Figure S5). In the 30 ppmv SO_2 scenario, ozone is decimated almost completely already at around 2 minutes after plume release, causing a temporarily decrease of BrX followed by an increase while the ozone concentration recovers. With a quenching to 6 ppm SO_2, which actually corresponds to the measured value, sufficient O_3 is provided which results in the almost complete reaction of Br radicals to other BrX species. The scenarios with 300 and 500 ppmv SO_2 show a rather complete depletion of ozone during the simulation time, but are not very realistic. A dilution time of 10 minutes (to a factor of 1/e (0.37) of the initial SO_2 mixing ratio) fits best to the measured average SO_2 mixing ratios in the aged plume.

With an initial magmatic H_XO_Y/NO_X abundance r-Br consists of less Br radicals and more other BrX species. The presence of NO_X (Figure S5) promotes the formation of reactive bromine reservoir species and causes less ozone consumption compared to the atmospheric H_XO_Y/NO_X case. The aerosol number concentration (NC) at a given aerosol size affects the Br activation. After reaching a certain threshold enough aerosol particles are present such that the Br activation is not limited by this parameter. This is also true for the radius of the aerosol particles at the number concentration of the base run. Regarding the base run scenario, a surface area of 3.4×10^{-3} m²/m^3 (3×10^9 particles m^{-3} at 300 nm radius) appears to be appropriate for the observed Br activation. Otherwise, less particles with the same radius leads to a slower activation similar to the same number of smaller particles. However, a larger surface area per volume leads to an increased activation pace. Similar to our observations Roberts et al. (2014) showed the impact of higher and lower aerosol surface on the Br activation, leading to larger and smaller activation respectively, in their PlumeChem model. However, the necessary surface area is easily provided by the volcanic aerosol at Masaya considering the obtained optical particle counter data on the particle sizes and abundances, which reached up to approximately 1.5×10^{-2} m²/m^3 calculated with data from Stix et al. (2018), so about 5 times as much as used in our base run scenario.

5.4.3. Chlorine and iodine chemistry

The HSC model produces reactive chlorine and iodine species. A typical output for chlorine is a Cl_2/Cl ratio of 8×10^{-5} and ClO/Cl of 3×10^{-6}. $ClONO_2$ and OClO are formed over the model run time and the measured reactive chlorine species are in the order of the model predictions (~0.3×10^{-3} at 2-3 minutes), although the model base run shows a decrease of reactive species during the first 7-8 minutes (see Figure 9).

Regarding iodine, the modelled speciation reflects the field observations, albeit only partially. Similar to Martin et al. (2006), 99 % of the iodine is present as atomic I in the HSC model. Diatomic iodine species are formed during the first minute of the box model simulation alongside HOI by reactions of analogous to R1 and R2. Eventually IO is further oxidized similar to R8 to form OIO, which is known to condense on preexisting particles and undergo new particle formation (e.g., Hoffmann et al., 2001; O'Dowd et al., 2002; Saiz-Lopez et al., 2012). CAABA/MECCA assumes a loss rate of OIO for new particle formation and uptake on existing aerosol that is combined to $I_XO_{Y(aq)}$. The kinetics of this process and the fate of the respective iodine species are not constrained very well. However, our measurements suggest a reactive iodine fraction (IX: I_2, IO, INO_2, $IONO_2$, HOI, OIO, HIO_3, ICl, IBr; r-I: IX + I) of 0.32±0.15 (0.16 to 0.70) at the crater rim which is in agreement with the model result and despite the high conversion of HI emission into reactive iodine, there is a low proportion (~ 4 %) of reactive iodine as IO. For a more distant position the measurements and the model diverge (Figure 9c), though potentially a smaller loss rate of OIO and further aqueous chemistry of $I_XO_{Y(aq)}$ could explain the measured reactive iodine species downwind. Furthermore, ultrafine and newly formed particles (<10nm) consisting of I_XO_Y could also diffuse to the denuder walls and react with the coating and therefore induce a false reactive iodine signal.

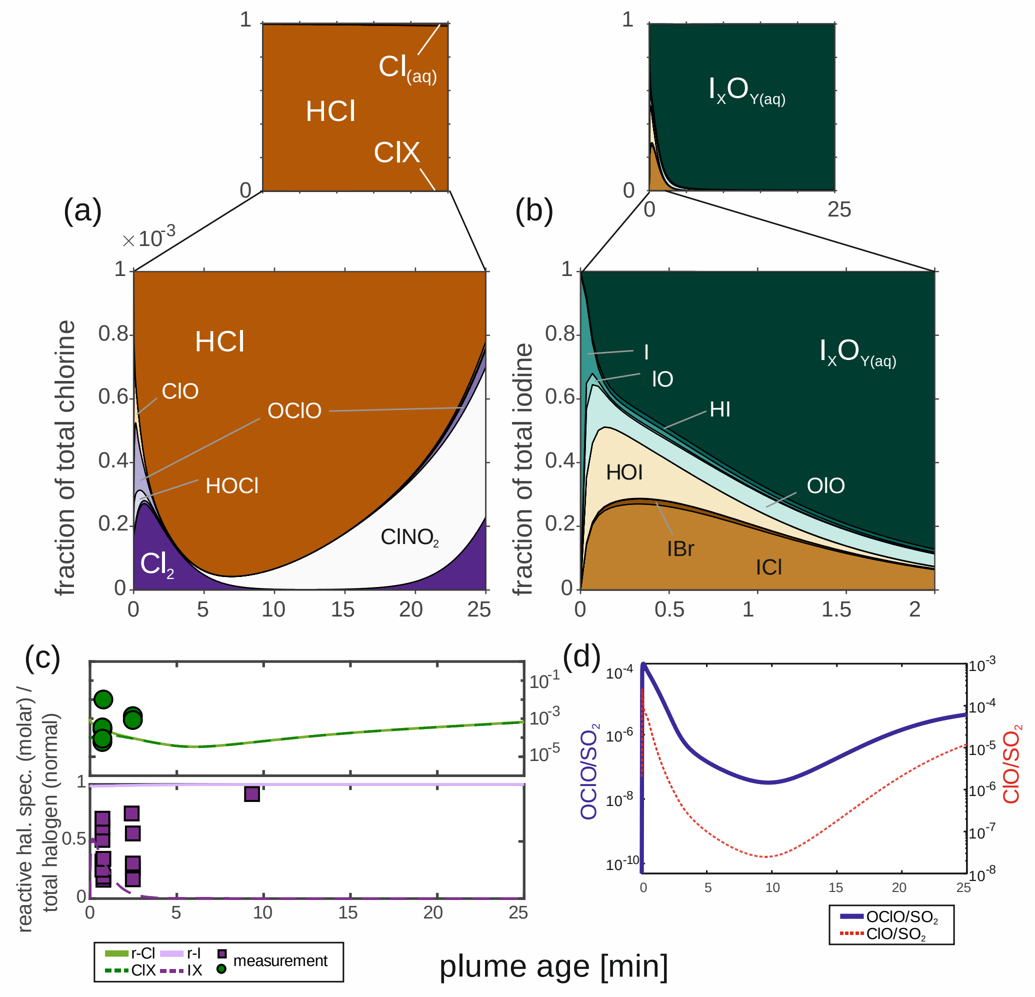

Figure 9: (a) Chlorine and **(b)** iodine speciation of the base model run (10:90 | 30 ppmv SO_2 | air | 10 min | 3×10^9 part. m^{-3} | $r = 3\times10^{-7}$ m); **(c)** comparison of the measured and modelled reactive halogen to total; **(d)** molar $OClO/SO_2$ and ClO/SO_2 ratios.

6. Conclusion and outlook

In this study, we present an innovative approach using a combination of ground-based and UAV-based measurements of halogen speciation in the plume of Masaya volcano over an estimated plume age of 1-11 minutes. Only by using an UAV we were enabled to sample the plume at an age that is typically not accessible. Additionally, the application of different techniques allowed the most detailed observation of changes in the halogen speciation during the first 11 minutes after the gas release. This led us to new observations: 1) the quantification of reactive bromine in the plume of Masaya at different plume ages, 2) the first quantification of reactive iodine and chlorine in the volcanic plume of Masaya. In addition, we provide the largest complementary data set to specify different halogen compounds at a volcano. These include alkaline traps (total amount of halogens), denuders (quantification of reactive halogens) and DOAS data (BrO), the latter two being applied to different plume ages. With these data, we finally succeeded in demonstrating through field studies that a large part of the emitted bromine is converted into reactive species (76 % already after 11.1 min), which was previously only assumed by model studies. The proportion of BrO (about 10%) to total bromine and the behavior of BrO/SO_2 to rapidly reach a plateau is in line with earlier studies (e.g. Gutmann et al, 2018). We have also shown that also a large part of iodine, namely 92%, is converted into reactive iodine compounds and that only a very small fraction, about 0.1%, of chlorine is converted into reactive chlorine.

In addition to our field studies we applied the CAABA/MECCA box model to test, if our current understanding of bromine chemistry in volcanic plumes fits our experimental results, when assuming reasonable input data for the species not measured. The BrO contribution to r-Br, determined by measurement data, could be reproduced by our box model simulations. The overall progression of the BrX/Br and r-Br/Br ratios were reflected by various model runs encompassing different plausible starting parameters. Although the bromine activation was reproduced by CAABA/MECCA, differences of reactive bromine to sulfur ratios occurred between observations and model, which might be caused by underestimation of SO_2 in the electrochemical sensor data for the diluted plume. Alongside more detailed observational studies, extension of knowledge on the chemical mechanisms of reactions occurring in volcanic plume environments is still needed. The knowledge of further data on O_3, H_XO_Y and NO_X in the plume would help to pin point a more detailed set of start parameters. The measured and modelled chlorine speciation are comparable. For iodine the implementations of iodine chemistry such as the knowledge on iodine oxide particle formation into the model are necessary to enable a qualified comparison with the observed iodine data. Within the range of model parameters that we studied, the dilution time and the quenching factor were shown to have a large effect on the plume chemistry while the initial volume ratio of atmospheric and magmatic gases (in the HSC model) seems to play only a less important role. The presence of initial oxidants showed to influence the relative abundance of the single Br species (e.g., Br_2, BrCl, $BrNO_3$, BrO, Br), while not largely affecting the overall reactive bromine abundance.

Our method achieved to determine the sum of reactive species for the respective halogens, which presents an important achievement for our knowledge on volcanic plume halogen chemistry. But more detailed speciation within the reactive fraction is a desirable topic of future research. For this purpose, other selective denuder coatings will be developed and applied to further distinguish between species such as Br_2, BrCl or $BrNO_3$ and Br radicals. Although we estimated that BrO contributes up to 10 % of r-Br and r-Br accounts for up to 76% of total Br after 10 minutes, the BrO formation seems to be more sensitive to changing model parameters than the overall r-Br formation. Since BrO detection is possible with DOAS spectrometers and has already been conducted at numerous volcanoes, the influencing factors on the extent of its formation need to be studied further, in particular with its potential as volcanic forecasting parameter and its use to estimate total bromine emissions. Detailed measurements in the field and further studies in controlled environments like atmospheric simulation chambers will help to further assess bromine activation in volcanic plumes.

Author contributions.

JR, NB and TH designed the research. JR, AG, NB, JMdM, MI, MM, AF and JS performed field sample and data collection. JR, AG, ML conducted laboratory sample analyses. FD provided the BrO/SO_2 NOVAC results. JR, JLT, AS, EM, JV and JMC provided instrumental and logistical support. RS provided the CAABA/MECCA program and helped to perform model runs. All authors contributed to the manuscript.

Competing interests

The authors declare that they have no conflict of interest.

Acknowledgments

JR, NB, AG and TH acknowledge support by the research center “Volcanoes and Atmosphere in Magmatic, Open Systems” (VAMOS) at the University of Mainz, Germany. JR is thankful for funding from the German Academic Exchange Service (DAAD) and the support by INETER (Nicaragua) and OVSICORI Universidad Nacional (Costa Rica). JR and NB thank also the DFG project “HALVIRE” (BO 3611/2-1, HE 5214/8-1, PL 193/18-1) for financial support during data evaluation, modelling and writing. Our thanks also to Dr. Feiyue Wang from the Centre for Earth Observation Science (CEOS) and the Department of Environment and Geography of the University of Manitoba Canada, for supporting field work at the Masaya complex. We would like to thank the referees Christoph Kern, Tjarda Roberts and the anonymous referee for their comprehensive reviews that helped to improve the manuscript substantially.

References

Aiuppa, A.: Degassing of halogens from basaltic volcanism: Insights from volcanic gas observations, Chemical Geology, 263, 99–109, doi:10.1016/j.chemgeo.2008.08.022, 2009.

Aiuppa, A., Baker, D. R., and Webster, J. D.: Halogens in volcanic systems, Chemical Geology, 263, 1–18, doi:10.1016/j.chemgeo.2008.10.005, 2009.

Aiuppa, A., Federico, C., Franco, A., Giudice, G., Gurrieri, S., Inguaggiato, S., Liuzzo, M., McGonigle, A. J. S., and Valenza, M.: Emission of bromine and iodine from Mount Etna volcano, Geochemistry, Geophysics, Geosystems, 6, n/a-n/a, doi:10.1029/2005GC000965, 2005.

Aiuppa, A., Federico, C., Giudice, G., Gurrieri, S., Liuzzo, M., Shinohara, H., Favara, R., and Valenza, M.: Rates of carbon dioxide plume degassing from Mount Etna volcano, Journal of Geophysical Research: Solid Earth, 111, doi:10.1029/2006JB004307, 2006.

Aiuppa, A., Moor, J. M. de, Arellano, S., Coppola, D., Francofonte, V., Galle, B., Giudice, G., Liuzzo, M., Mendoza, E., Saballos, A., Tamburello, G., Battaglia, A., Bitetto, M., Gurrieri, S., Laiolo, M., Mastrolia, A., and Moretti, R.: Tracking Formation of a Lava Lake From Ground and Space: Masaya Volcano (Nicaragua), 2014-2017, Geochemistry, Geophysics, Geosystems, 19, 496–515, doi:10.1002/2017GC007227, 2018.

Aiuppa, A., Moretti, R., Federico, C., Giudice, G., Gurrieri, S., Liuzzo, M., Papale, P., Shinohara, H., and Valenza, M.: Forecasting Etna eruptions by real-time observation of volcanic gas composition, Geology, 35, 1115–1118, doi:10.1130/G24149A.1, 2007.

Bobrowski, N. and Giuffrida, G.: Bromine monoxide/sulphur dioxide ratios in relation to volcanological observations at Mt. Etna 2006-2009, Solid Earth, 3, 433, 2012.

Bobrowski, N., Giuffrida, G. B., Arellano, S., Yalire, M., Liotta, M., Brusca, L., Calabrese, S., Scaglione, S., Rüdiger, J., Castro, J. M., Galle, B., and Tedesco, D.: Plume composition and volatile flux of Nyamulagira volcano, Democratic Republic of Congo, during birth and evolution of the lava lake, 2014–2015, Bulletin of Volcanology, 79, B09207, doi:10.1007/s00445-017-1174-0, 2017.

Bobrowski, N., Glasow, R. von, Aiuppa, A., Inguaggiato, S., Louban, I., Ibrahim, O. W., and Platt, U.: Reactive halogen chemistry in volcanic plumes, Journal of Geophysical Research, 112, doi:10.1029/2006JD007206, 2007.

Bobrowski, N., Hönninger, G., Galle, B., and Platt, U.: Detection of bromine monoxide in a volcanic plume, Nature, 423, 273–276, 2003.

Bobrowski, N. and Platt, U.: SO2/BrO ratios studied in five volcanic plumes, Journal of Volcanology and Geothermal Research, 166, 147–160, 2007.

Bryukov, M. G., Slagle, I. R., and Knyazev, V. D.: Kinetics of Reactions of Cl Atoms with Methane and Chlorinated Methanes, The Journal of Physical Chemistry A, 106, 10532–10542, doi:10.1021/jp0257909, 2002.

Burton, M. R., Oppenheimer, C., Horrocks, L. A., and Francis, P. W.: Remote sensing of CO2 and H2O emission rates from Masaya volcano, Nicaragua, Geology, 28, 915–918, doi:10.1130/0091-7613(2000)28<915:RSOCAH>2.0.CO;2, 2000.

Burton, M. R., Mader, H. M., and Polacci, M.: The role of gas percolation in quiescent degassing of persistently active basaltic volcanoes, Earth and Planetary Science Letters, 264, 46–60, doi:10.1016/j.epsl.2007.08.028, 2007.

Cadoux, A., Iacono-Marziano, G., Scaillet, B., Aiuppa, A., Mather, T. A., Pyle, D. M., Deloule, E., Gennaro, E., and Paonita, A.: The role of melt composition on aqueous fluid vs. silicate melt partitioning of bromine in magmas, Earth and Planetary Science Letters, 498, 450–463, doi:10.1016/j.epsl.2018.06.038, 2018.

Carn, S. A., Clarisse, L., and Prata, A. J.: Multi-decadal satellite measurements of global volcanic degassing, Journal of Volcanology and Geothermal Research, 311, 99–134, doi:10.1016/j.jvolgeores.2016.01.002, 2016.

Carn, S. A., Fioletov, V. E., McLinden, C. A., Li, C., and Krotkov, N. A.: A decade of global volcanic SO2 emissions measured from space, Scientific reports, 7, 44095, doi:10.1038/srep44095, 2017.

Carn, S. A., Froyd, K. D., Anderson, B. E., Wennberg, P., Crounse, J., Spencer, K., Dibb, J. E., Krotkov, N. A., Browell, E. V., Hair, J. W., Diskin, G., Sachse, G., and Vay, S. A.: In situ measurements of tropospheric volcanic plumes in Ecuador and Colombia during TC 4, Journal of Geophysical Research, 116, 86, doi:10.1029/2010JD014718, 2011.

Carroll, R. and Holloway, J. R.: Volatiles in magmas, Reviews in mineralogy, op. 1994.

de Moor, J. M., Aiuppa, A., Avard, G., Wehrmann, H., Dunbar, N., Muller, C., Tamburello, G., Giudice, G., Liuzzo, M., Moretti, R., Conde, V., and Galle, B.: Turmoil at Turrialba Volcano (Costa Rica): Degassing and eruptive processes inferred from high-frequency gas monitoring, Journal of geophysical research. Solid earth, 121, 5761–5775, doi:10.1002/2016JB013150, 2016.

de Moor, J. M., Fischer, T. P., Sharp, Z. D., King, P. L., Wilke, M., Botcharnikov, R. E., Cottrell, E., Zelenski, M., Marty, B., Klimm, K., Rivard, C., Ayalew, D., Ramirez, C., and Kelley, K. A.: Sulfur degassing at Erta Ale (Ethiopia) and Masaya (Nicaragua) volcanoes: Implications for degassing processes and oxygen fugacities of basaltic systems, Geochemistry, Geophysics, Geosystems, 14, 4076–4108, doi:10.1002/ggge.20255, 2013.

de Moor, J. M., Kern, C., Avard, G., Muller, C., Aiuppa, A., Saballos, A., Ibarra, M., LaFemina, P., Protti, M., and Fischer, T. P.: A New Sulfur and Carbon Degassing Inventory for the Southern Central American Volcanic Arc: The Importance of Accurate Time-Series Datasets and Possible Tectonic Processes Responsible for Temporal Variations in Arc-Scale Volatile Emissions, Geochemistry, Geophysics, Geosystems, doi:10.1002/2017GC007141, 2017.

Delmelle, P., Stix, J., Baxter, P., Garcia-Alvarez, J., and Barquero, J.: Atmospheric dispersion, environmental effects and potential health hazard associated with the low-altitude gas plume of Masaya volcano, Nicaragua, Bulletin of Volcanology, 64, 423–434, doi:10.1007/s00445-002-0221-6, 2002.

Delmelle, P.: Environmental impacts of tropospheric volcanic gas plumes, Geological Society, London, Special Publications, 213, 381–399, doi:10.1144/GSL.SP.2003.213.01.23, 2003.

Diaz, J. A., Pieri, D., Wright, K., Sorensen, P., Kline-Shoder, R., Arkin, C. R., Fladeland, M., Bland, G., Buongiorno, M. F., Ramirez, C., Corrales, E., Alan, A., Alegria, O., Diaz, D., and Linick, J.: Unmanned aerial mass spectrometer systems for in-situ volcanic plume analysis, Journal of the American Society for Mass Spectrometry, 26, 292–304, doi:10.1007/s13361-014-1058-x, 2015.

Dinger, F., Bobrowski, N., Warnach, S., Bredemeyer, S., Hidalgo, S., Arellano, S., Galle, B., Platt, U., and Wagner, T.: Periodicity in the BrO⁄SO2; molar ratios in the volcanic gas plume of Cotopaxi and its correlation with the Earth tides during the eruption in 2015, Solid Earth, 9, 247–266, doi:10.5194/se-9-247-2018, 2018.

Dinger, F.: On long-term variations in the BrO/SO2 molar ratios in volcanic gas plumes, Johannes Gutenberg-University Mainz, 2019. https://publications.ub.uni-mainz.de/theses/frontdoor.php?source_opus=100003100&la=de

Donovan, A., Tsanev, V., Oppenheimer, C., and Edmonds, M.: Reactive halogens (BrO and OClO) detected in the plume of Soufrière Hills Volcano during an eruption hiatus, Geochemistry Geophysics Geosystems, 15, 3346–3363, doi:10.1002/2014GC005419, 2014.

Duffell, H. J., Oppenheimer, C., Pyle, D. M., Galle, B., McGonigle, A. J.S., and Burton, M. R.: Changes in gas composition prior to a minor explosive eruption at Masaya volcano, Nicaragua, Journal of Volcanology and Geothermal Research, 126, 327–339, doi:10.1016/S0377-0273(03)00156-2, 2003.

Fickert, S., Adams, J. W., and Crowley, J. N.: Activation of Br2 and BrCl via uptake of HOBr onto aqueous salt solutions, Journal of Geophysical Research: Atmospheres, 104, 23719–23727, doi:10.1029/1999JD900359, 1999.

Galle, B., Johansson, M., Rivera, C., Zhang, Y., Kihlman, M., Kern, C., Lehmann, T., Platt, U., Arellano, S., and Hidalgo, S.: Network for Observation of Volcanic and Atmospheric Change (NOVAC)—A global network for volcanic gas monitoring: Network layout and instrument description, Journal of Geophysical Research, 115, 151, doi:10.1029/2009JD011823, 2010.

General, S., Bobrowski, N., Pöhler, D., Weber, K., Fischer, C., and Platt, U.: Airborne I-DOAS measurements at Mt. Etna: BrO and OClO evolution in the plume, Journal of Volcanology and Geothermal Research, 300, 175–186, doi:10.1016/j.jvolgeores.2014.05.012, 2015.

Gerlach, T. M.: Volcanic sources of tropospheric ozone-depleting trace gases, Geochemistry, Geophysics, Geosystems, 5,, doi:10.1029/2004GC000747, 2004.

Giggenbach, W. F.: Variations in the carbon, sulfur and chlorine contents of volcanic gas discharges from White Island, New Zealand, Bulletin of Volcanology, 39, 15–27, doi:10.1007/BF02596943, 1975.

Gliß, J., Bobrowski, N., Vogel, L., Pöhler, D., and Platt, U.: OClO and BrO observations in the volcanic plume of Mt. Etna – implications on the chemistry of chlorine and bromine species in volcanic plumes, Atmospheric Chemistry and Physics, 15, 5659–5681, doi:10.5194/acp-15-5659-2015, 2015.

Gutmann, A., Bobrowski, N., Roberts, T., Rüdiger, J., and Hoffmann, T.: Advances in bromine speciation in volcanic plumes, Front. Earth Sci., 6, 213, doi:10.3389/feart.2018.00213, 2018.

Heue, K.-P., Brenninkmeijer, C. A. M., Baker, A. K., Rauthe-Schöch, A., Walter, D., Wagner, T., Hörmann, C., Sihler, H., Dix, B., Frieß, U., Platt, U., Martinsson, B. G., van Velthoven, P. F. J., Zahn, A., and Ebinghaus, R.: SO_2 and BrO observation in the plume of the Eyjafjallajökull volcano 2010: CARIBIC and GOME-2 retrievals, Atmos. Chem. Phys., 11, 2973–2989, doi:10.5194/acp-11-2973-2011, 2011.

Hippler, H. and Troe, J.: Flash photolysis study of the recombination of chlorine atoms in the presence of various inert gases and NO, International journal of chemical kinetics, 8, 501–510, doi:10.1002/kin.550080404, 1976.

Hobbs, P. V., Tuell, J. P., Hegg, D. A., Radke, L. F., and Eltgroth, M. W.: Particles and gases in the emissions from the 1980–1981 volcanic eruptions of Mt. St. Helens, Journal of Geophysical Research, 87, 11062, doi:10.1029/JC087iC13p11062, 1982.

Hoffmann, T., O'Dowd, C. D., and Seinfeld, J. H.: Iodine oxide homogeneous nucleation: An explanation for coastal new particle production, Geophysical Research Letters, 28, 1949–1952, doi:10.1029/2000GL012399, 2001.

Huff, A. K. and Abbatt, J. P. D.: Gas-Phase Br 2 Production in Heterogeneous Reactions of Cl 2 HOCl, and BrCl with Halide−Ice Surfaces, The Journal of Physical Chemistry A, 104, 7284–7293, doi:10.1021/jp001155w, 2000.

Iowa State University: Iowa Environmental Mesonet: ASOS-AWOS-METAR Data: https://mesonet.agron.iastate.edu/request/download.phtml?network=NI__ASOS, last access: 20 October 2018.

Jourdain, L., Roberts, T. J., Pirre, M., and Josse, B.: Modeling the reactive halogen plume from Ambrym and its impact on the troposphere with the CCATT-BRAMS mesoscale model, Atmospheric Chemistry and Physics, 16, 12099–12125, doi:10.5194/acp-16-12099-2016, 2016.

Kelly, P. J., Kern, C., Roberts, T. J., Lopez, T., Werner, C., and Aiuppa, A.: Rapid chemical evolution of tropospheric volcanic emissions from Redoubt Volcano, Alaska, based on observations of ozone and halogen-containing gases, Journal of Volcanology and Geothermal Research, 259, 317–333, doi:10.1016/j.jvolgeores.2012.04.023, 2013.

Kern, C. and Lyons, J. J.: Spatial distribution of halogen oxides in the plume of Mount Pagan volcano, Mariana Islands, Geophysical Research Letters, doi:10.1029/2018GL079245, 2018.

Kern, C., Sihler, H., Vogel, L., Rivera, C., Herrera, M., and Platt, U.: Halogen oxide measurements at Masaya Volcano, Nicaragua using active long path differential optical absorption spectroscopy, Bulletin of Volcanology, 71, 659–670, doi:10.1007/s00445-008-0252-8, 2009.

Laaksonen, A., Korhonen, P., Kulmala, M., and Charlson, R. J.: Modification of the Köhler Equation to Include Soluble Trace Gases and Slightly Soluble Substances, Journal of the Atmospheric Sciences, 55, 853–862, doi:10.1175/1520-0469(1998)055<0853:MOTKHE>2.0.CO;2, 1998.

Lee, C., Kim, Y. J., Tanimoto, H., Bobrowski, N., Platt, U., Mori, T., Yamamoto, K., and Hong, C. S.: High ClO and ozone depletion observed in the plume of Sakurajima volcano, Japan, Geophysical Research Letters, 32, 2005.

Liotta, M., Rizzo, A., Paonita, A., Caracausi, A., and Martelli, M.: Sulfur isotopic compositions of fumarolic and plume gases at Mount Etna (Italy) and inferences on their magmatic source, Geochemistry Geophysics Geosystems, 13, doi:10.1029/2012GC004118, 2012.

Louban, I., Bobrowski, N., Rouwet, D., Inguaggiato, S., and Platt, U.: Imaging DOAS for volcanological applications, Bulletin of Volcanology, 71, 753–765, doi:10.1007/s00445-008-0262-6, 2009.

Lübcke, P., Bobrowski, N., Arellano, S., Galle, B., Garzón, G., Vogel, L., and Platt, U.: BrO/SO$_2$ molar ratios from scanning DOAS measurements in the NOVAC network, Solid Earth, 5, 409–424, doi:10.5194/se-5-409-2014, 2014.

Malavelle, F. F., Haywood, J. M., Jones, A., Gettelman, A., Clarisse, L., Bauduin, S., Allan, R. P., Karset, I. H. H., Kristjánsson, J. E., Oreopoulos, L., Cho, N., Lee, D., Bellouin, N., Boucher, O., Grosvenor, D. P., Carslaw, K. S., Dhomse, S., Mann, G. W., Schmidt, A., Coe, H., Hartley, M. E., Dalvi, M., Hill, A. A., Johnson, B. T., Johnson, C. E., Knight, J. R., O'Connor, F. M., Partridge, D. G., Stier, P., Myhre, G., Platnick, S., Stephens, G. L., Takahashi, H., and Thordarson, T.: Strong constraints on aerosol–cloud interactions from volcanic eruptions, Nature, 546, 485, doi:10.1038/nature22974, 2017.

Maric et al.: A study of the UV—visible absorption spectra of Br2 and BrCl, Journal of Photochemistry and Photobiology A: Chemistry, 83, 179–192, doi:10.1016/1010-6030(94)03823-6, 1994.

Martin, R. S., Mather, T. A., and Pyle, D. M.: High-temperature mixtures of magmatic and atmospheric gases, Geochemistry, Geophysics, Geosystems, 7, doi:10.1029/2005GC001186, 2006.

Martin, R. S., Sawyer, G. M., Spampinato, L., Salerno, G. G., Ramirez, C., Ilyinskaya, E., Witt, M. L. I., Mather, T. A., Watson, I. M., Phillips, J. C., and Oppenheimer, C.: A total volatile inventory for Masaya Volcano, Nicaragua, Journal of Geophysical Research, 115, doi:10.1029/2010JB007480, 2010.

Martin, R. S., Ilyinskaya, E., and Oppenheimer, C.: The enigma of reactive nitrogen in volcanic emissions, Geochimica et Cosmochimica Acta, 95, 93–105, doi:10.1016/j.gca.2012.07.027, 2012

Mather, T. A., Pyle, D. M., and Oppenheimer, C.: Tropospheric Volcanic Aerosol, American Geophysical Union (AGU), 189 pp., doi:10.1029/139GM12: https://agupubs.onlinelibrary.wiley.com/doi/full/10.1029/139GM12, 2013.

McBirney, A. R.: The Nicaraguan volcano Masaya and its caldera, Transactions, American Geophysical Union, 37, 83, doi:10.1029/TR037i001p00083, 1956.

McGonigle, A. J. S., Aiuppa, A., Giudice, G., Tamburello, G., Hodson, A. J., and Gurrieri, S.: Unmanned aerial vehicle measurements of volcanic carbon dioxide fluxes, Geophysical Research Letters, 35, doi:10.1029/2007GL032508, 2008.

McGonigle, A. J. S., Delmelle, P., Oppenheimer, C., Tsanev, V. I., Delfosse, T., Williams-Jones, G., Horton, K., and Mather, T. A.: SO2 depletion in tropospheric volcanic plumes, Geophysical Research Letters, 31, doi:10.1029/2004GL019990, 2004.

Mori, T., Hashimoto, T., Terada, A., Yoshimoto, M., Kazahaya, R., Shinohara, H., and Tanaka, R.: Volcanic plume measurements using a UAV for the 2014 Mt. Ontake eruption, Earth, Planets and Space, 68, 1861, doi:10.1186/s40623-016-0418-0, 2016.

Noguchi, K. and Kamiya, H.: Prediction of volcanic eruption by measuring the chemical composition and amounts of gases, Bulletin of Volcanology, 26, 367–378, doi:10.1007/BF02597298, 1963.

O'Dowd, C. D., Jimenez, J. L., Bahreini, R., Flagan, R. C., Seinfeld, J. H., Hämeri, K., Pirjola, L., Kulmala, M., Jennings, S. G., and Hoffmann, T.: Marine aerosol formation from biogenic iodine emissions, Nature, 417, 632, doi:10.1038/nature00775, 2002.

Oppenheimer, C., Kyle, P., Eisele, F., Crawford, J., Huey, G., Tanner, D., Kim, S., Mauldin, L., Blake, D., Beyersdorf, A., Buhr, M., and Davis, D.: Atmospheric chemistry of an Antarctic volcanic plume, Journal of Geophysical Research, 115, 5473, doi:10.1029/2009JD011910, 2010.

Oppenheimer, C., Tsanev, V. I., Braban, C. F., Cox, R. A., Adams, J. W., Aiuppa, A., Bobrowski, N., Delmelle, P., Barclay, J., and McGonigle, A. J.S.: BrO formation in volcanic plumes, Geochimica et Cosmochimica Acta, 70, 2935–2941, doi:10.1016/j.gca.2006.04.001, 2006.

Platt, U. and Bobrowski, N.: Quantification of volcanic reactive halogen emissions, in: Volcanism and global environmental change, Schmidt, A., Fristad, K., and Elkins-Tanton, L. T. (Eds.), Cambridge University Press, Cambridge, 115–132, 2015.

Platt, U. and Stutz, J.: Differential absorption spectroscopy, in: Differential Optical Absorption Spectroscopy, Springer, 135–174, 2008.

Pyle, D. M. and Mather, T. A.: Halogens in igneous processes and their fluxes to the atmosphere and oceans from volcanic activity: A review, Chemical Geology, 263, 110–121, doi:10.1016/j.chemgeo.2008.11.013, 2009.

Roberts, T.: Ozone Depletion in Tropospheric Volcanic Plumes: From Halogen-Poor to Halogen-Rich Emissions, Geosciences, 8, 68, doi:10.3390/geosciences8020068, 2018.

Roberts, T. J., Braban, C. F., Martin, R. S., Oppenheimer, C., Adams, J. W., Cox, R. A., Jones, R. L., and Griffiths, P. T.: Modelling reactive halogen formation and ozone depletion in volcanic plumes, Chemical Geology, 263, 151–163, doi:10.1016/j.chemgeo.2008.11.012, 2009.

Roberts, T. J., Martin, R. S., and Jourdain, L.: Reactive bromine chemistry in Mount Etna’s volcanic plume: The influence of total Br, high-temperature processing, aerosol loading and plume–air mixing, Atmospheric Chemistry and Physics, 14, 11201–11219, doi:10.5194/acp-14-11201-2014, 2014.

Roberts, T. J., Vignelles, D., Liuzzo, M., Giudice, G., Aiuppa, A., Coltelli, M., Salerno, G., Chartier, M., Couté, B., Berthet, G., Lurton, T., Dulac, F., and Renard, J.-B.: The primary volcanic aerosol emission from Mt Etna: Size-resolved particles with SO 2 and role in plume reactive halogen chemistry, Geochimica et Cosmochimica Acta, 222, 74–93, doi:10.1016/j.gca.2017.09.040, 2018.

Roberts, T., Dayma, G., and Oppenheimer, C.: Reaction Rates Control High-Temperature Chemistry of Volcanic Gases in Air, Front. Earth Sci., 7, 1441, doi:10.3389/feart.2019.00154, 2019.

Rose, W. I., Millard, G. A., Mather, T. A., Hunton, D. E., Anderson, B., Oppenheimer, C., Thornton, B. F., Gerlach, T. M., Viggiano, A. A., Kondo, Y., Miller, T. M., and Ballenthin, J. O.: Atmospheric chemistry of a 33–34 hour old volcanic cloud from Hekla Volcano (Iceland): Insights from direct sampling and the application of chemical box modeling, Journal of Geophysical Research, 111, Q08008, doi:10.1029/2005JD006872, 2006.

Rüdiger, J., Bobrowski, N., Liotta, M., and Hoffmann, T.: Development and application of a sampling method for the determination of reactive halogen species in volcanic gas emissions, Analytical and bioanalytical chemistry, 52, 325, doi:10.1007/s00216-017-0525-1, 2017.

Rüdiger, J., Tirpitz, J.-L., Moor, J. M. de, Bobrowski, N., Gutmann, A., Liuzzo, M., Ibarra, M., and Hoffmann, T.: Implementation of electrochemical, optical and denuder-based sensors and sampling techniques on UAV for volcanic gas measurements: Examples from Masaya, Turrialba and Stromboli volcanoes, Atmospheric Measurement Techniques, 11, 2441–2457, doi:10.5194/amt-11-2441-2018, 2018.

Saiz-Lopez, A. and von Glasow, R.: Reactive halogen chemistry in the troposphere, Chemical Society reviews, 41, 6448–6472, doi:10.1039/c2cs35208g, 2012.

Saiz-Lopez, A., Plane, J. M. C., Baker, A. R., Carpenter, L. J., Glasow, R. v., Martín, J. C. G., McFiggans, G., and Saunders, R. W.: Atmospheric chemistry of iodine, Chemical reviews, 112, 1773–1804, doi:10.1021/cr200029u, 2012.

Sander, R., Baumgaertner, A., Gromov, S., Harder, H., Jöckel, P., Kerkweg, A., Kubistin, D., Regelin, E., Riede, H., Sandu, A., Taraborrelli, D., Tost, H., and Xie, Z.-Q.: The atmospheric chemistry box model CAABA/MECCA-3.0, Geoscientific Model Development, 4, 373–380, doi:10.5194/gmd-4-373-2011, 2011.

Sander, R., Jöckel, P., Kirner, O., Kunert, A. T., Landgraf, J., and Pozzer, A.: The photolysis module JVAL-14, compatible with the MESSy standard, and the JVal PreProcessor (JVPP), Geosci. Model Dev., 7, 2653–2662, doi:10.5194/gmd-7-2653-2014, 2014.

Schönhardt, A., Richter, A., Theys, N., and Burrows, J. P.: Space-based observation of volcanic iodine monoxide, Atmospheric Chemistry and Physics, 17, 4857–4870, doi:10.5194/acp-17-4857-2017, 2017.

Shinohara, H.: A new technique to estimate volcanic gas composition: Plume measurements with a portable multi-sensor system, Journal of Volcanology and Geothermal Research, 143, 319–333, doi:10.1016/j.jvolgeores.2004.12.004, 2005.

Simpson, W. R., Glasow, R. von, Riedel, K., Anderson, P., Ariya, P., Bottenheim, J., Burrows, J., Carpenter, L. J., Frieß, U., Goodsite, M. E., Heard, D., Hutterli, M., Jacobi, H.-W., Kaleschke, L., Neff, B., Plane, J., Platt, U., Richter, A., Roscoe, H., Sander, R., Shepson, P., Sodeau, J., Steffen, A., Wagner, T., and Wolff, E.: Halogens and their role in polar boundary-layer ozone depletion, Atmospheric Chemistry and Physics, 7, 4375–4418, doi:10.5194/acp-7-4375-2007, 2007.

Stix, J., de Moor, J. M. de, Rüdiger, J., Alan, A., Corrales, E., D'Arcy, F., Diaz, J. A., and Liotta, M.: Using Drones and Miniaturized Instrumentation to Study Degassing at Turrialba and Masaya Volcanoes, Central America, Journal of Geophysical Research: Solid Earth, doi:10.1029/2018JB015655, 2018.

Surl, L., Donohoue, D., Aiuppa, A., Bobrowski, N., and Glasow, R. von: Quantification of the depletion of ozone in the plume of Mount Etna, Atmospheric Chemistry and Physics, 15, 2613–2628, doi:10.5194/acp-15-2613-2015, 2015.

Symonds, R. B., Rose, W. I., Bluth, G. J. S., and Gerlach, T. M.: Volcanic-gas studies; methods, results, and applications, Reviews in Mineralogy and Geochemistry, 30, 1–66, 1994.

Theys, N., Smedt, I. de, van Roozendael, M., Froidevaux, L., Clarisse, L., and Hendrick, F.: First satellite detection of volcanic OClO after the eruption of Puyehue-Cordón Caulle, Geophysical Research Letters, 41, 667–672, doi:10.1002/2013GL058416, 2014.

Theys, N., van Roozendael, M., Dils, B., Hendrick, F., Hao, N., and Mazière, M. de: First satellite detection of volcanic bromine monoxide emission after the Kasatochi eruption, Geophysical Research Letters, 36, doi:10.1029/2008GL036552, 2009.

Vogel, L.: Volcanic plumes: Evaluation of spectroscopic measurements, early detection, and bromine chemistry, Heidelberg University Library, 2012.

van Manen, S. M.: Perception of a chronic volcanic hazard: Persistent degassing at Masaya volcano, Nicaragua, J Appl. Volcanol., 3, 155, doi:10.1186/s13617-014-0009-3, 2014.

von Glasow, R.: Atmospheric chemistry in volcanic plumes, Proceedings of the National Academy of Sciences of the United States of America, 107, 6594–6599, doi:10.1073/pnas.0913164107, 2010.

von Glasow, R., Bobrowski, N., and Kern, C.: The effects of volcanic eruptions on atmospheric chemistry, Chemical Geology, 263, 131–142, doi:10.1016/j.chemgeo.2008.08.020, 2009.

Weber, K., Eliasson, J., Vogel, A., Fischer, C., Pohl, T., van Haren, G., Meier, M., Grobéty, B., and Dahmann, D.: Airborne in-situ investigations of the Eyjafjallajökull volcanic ash plume on Iceland and over north-western Germany with light aircrafts and optical particle counters, Atmospheric Environment, 48, 9–21, doi:10.1016/j.atmosenv.2011.10.030, 2012.

Wennberg, P.: Atmospheric chemistry: Bromine explosion, Nature, 397, 299–301, 1999.

Witt, M. L. I., Mather, T. A., Pyle, D. M., Aiuppa, A., Bagnato, E., and Tsanev, V. I.: Mercury and halogen emissions from Masaya and Telica volcanoes, Nicaragua, Journal of Geophysical Research, 113, doi:10.1029/2007JB005401, 2008.

Wittmer, J., Bobrowski, N., Liotta, M., Giuffrida, G., Calabrese, S., and Platt, U.: Active alkaline traps to determine acidic-gas ratios in volcanic plumes: Sampling techniques and analytical methods, Geochemistry, Geophysics, Geosystems, 15, 2797–2820, doi:10.1002/2013GC005133, 2014.

References